# A Problem-Oriented Taxonomy of Evaluation Metrics for Time Series Anomaly Detection

Kaixiang Yang, Jiarong Liu, Yupeng Song, Shuanghua Yang, Senior Member, IEEE, and Yujue Zhou

Abstract-Time series anomaly detection is widely used in IoT and cyber-physical systems, yet its evaluation remains challenging due to diverse application objectives and heterogeneous metric assumptions. This study introduces a problem-oriented framework that reinterprets existing metrics based on the specific evaluation challenges they are designed to address, rather than their mathematical forms or output structures. We categorize over twenty commonly used metrics into six dimensions: (1) basic accuracydriven evaluation, (2) timeliness-aware reward mechanisms, (3) tolerance to labeling imprecision, (4) penalties reflecting humanaudit cost, (5) robustness against random or inflated scores, and (6) parameter-free comparability for cross-dataset benchmarking. Comprehensive experiments are conducted to examine metric behavior under genuine, random, and oracle detection scenarios. By comparing their resulting score distributions, we quantify each metric's discriminative ability—its capability to distinguish meaningful detections from random noise. The results show that while most event-level metrics exhibit strong separability, several widely used metrics (e.g., NAB, Point-Adjust) demonstrate limited resistance to random-score inflation. These findings reveal that metric suitability must be inherently task-dependent and aligned with the operational objectives of IoT applications. The proposed framework offers a unified analytical perspective for understanding existing metrics and provides practical guidance for selecting or developing more context-aware, robust, and fair evaluation methodologies for time series anomaly detection.

Index Terms—Time series anomaly detection, Time series, performance evaluation metrics, evaluation framework.

# I. Introduction

The emergence of the Internet of Things (IoT) has accelerated digital transformation across numerous domains. Its defining characteristic lies in the large-scale deployment of intelligent and heterogeneous devices—such as sensors, actuators, and RFID systems—that are interconnected via the Internet to enable autonomous communication without human intervention [1]. Currently, more than 12 billion IoT devices are in operation, and this number is projected to reach 125 billion by 2030 [2]. Consequently, the volume of data generated by these devices continues to soar, with an expected total of 79.4 ZB by 2025 [3]. In industrial contexts, the integration of IoT technologies has driven the ongoing Industry 4.0 revolution, emphasizing connectivity, automation, and intelligence. By incorporating data analytics, AI algorithms, industrial machines, and IoT sensors, Industry

Kaixiang Yang, Jiarong Liu, Yupeng Song, and Yujue Zhou are with the School of Artificial Intelligence, Yunnan University, Kunming 650091, China. Shuanghua Yang is with Beijing Normal University – Hong Kong Baptist University, Zhuhai 519087, China.

This work was supported in part by the Yunnan Fundamental Research Projects under Grant 202401AU070151, and in part by the Yunnan Provincial Science and Technology Talent and Platform Plan under Grant 202505AF350053.

Corresponding author: Yujue Zhou (email: zhouyujue@ynu.edu.cn).

4.0 aims to construct a highly efficient and intelligent industrial ecosystem.

As Industry 4.0 evolves, time series data—the foundation of intelligent monitoring and measurement—has been generated at an unprecedented rate. This surge underscores the urgent need for advanced analytical tools capable of accurately identifying anomalies within massive data streams. Beyond industrial systems, time series anomaly detection (TSAD) plays a crucial role in various application scenarios, such as climate modeling, cyber-physical infrastructures [4], transportation [5], online service systems [6], biological sciences [7], smart grids [8], energy consumption systems [9], healthcare [10], spacecraft telemetry [11] and financial services [12]. The rapid progress of machine learning has further fueled the evolution of TSAD methods, leading to increasingly sophisticated models with complex data dependencies and adaptive learning capabilities.

However, the evaluation of anomaly detection performance has not progressed at the same rate as the development of new algorithms. The choice of evaluation metric fundamentally determines how detection behavior is quantified, interpreted, and compared under different operational requirements. In practice, different IoT and cyber-physical applications place distinct priorities on what "good performance" means: some emphasize early detection to prevent cascading failures, others focus on robustness under noisy or uncertain labels, while resource-constrained systems may prioritize metrics that reflect human-in-the-loop inspection cost. As a result, each metric implicitly reflects a particular evaluation objective that it is designed to emphasize—yet this objective is rarely made explicit in existing studies.

Despite their importance, anomaly detection metrics are seldom examined from an objective-oriented and application-driven standpoint. Existing taxonomies typically group metrics by mathematical form, aggregation level (point-based vs. event-based), or thresholding scheme. While these classifications are descriptive, they do not reveal the underlying evaluation motivations. For reliable and interpretable assessment—especially in heterogeneous IoT environments—it is crucial to understand metrics as tools designed to answer specific performance questions: What aspect of detection does the metric emphasize? Under what conditions does it behave reliably? And what types of uncertainty or bias does it introduce?

To address this gap, this paper presents an applicationdriven reexamination and reclassification of anomaly detection evaluation metrics. Unlike traditional taxonomies that focus primarily on computational structure, our framework organizes metrics according to their underlying evaluation

objectives—the specific performance demands they are intended to capture. This objective-aware perspective enables a clearer understanding of how metrics relate to one another, how they align with diverse IoT application needs, and how they influence the interpretation of algorithmic performance. By framing anomaly detection evaluation around operational requirements, rather than purely mathematical definitions, this work offers practical and theoretically grounded guidance for selecting and designing metrics in time series anomaly detection. The main contributions of this paper are summarized as follows:

# 1) Objective-Oriented Reinterpretation of TSAD Metrics

We reinterpret existing time series anomaly detection (TSAD) metrics from the standpoint of measurement science, viewing each metric as a measurement instrument designed to quantify a specific performance aspect under uncertainty. This provides a theoretical foundation for understanding how metrics embody distinct measurement objectives and trade-offs.

## 2) Problem-Driven Classification Framework:

We propose a new taxonomy that categorizes metrics by the evaluation problems they aim to address—such as timeliness, label uncertainty, threshold dependence, and inspection cost—rather than by their mathematical formulation. This reframing bridges the gap between algorithmic evaluation and real-world IoT application requirements.

# 3) Comparative Analysis and Evaluation Insights:

Through systematic comparison and case studies, we show that different metrics can yield substantially different assessments even on the same prediction results. We analyze these discrepancies in terms of evaluation bias, sensitivity, and interpretability, demonstrating the necessity of aligning metric choice with application-level objectives.

# 4) Guidelines for Metric Selection and Future Metric Design:

Based on the proposed framework, we provide guidelines for selecting suitable metrics under different operational constraints, and discuss future directions for designing next-generation metrics that improve fairness, robustness, and consistency in TSAD evaluation across IoT scenarios.

#### II. BACKGROUND

This section introduces the fundamental concepts necessary for understanding the subsequent discussions, including the basic formulation of time series anomaly detection tasks, the standard evaluation pipeline, and the classification framework of evaluation metrics.

# A. Time Series Anomaly Detection (TSAD) and Evaluation

1) Task Definition and Output Form: A time series is a sequence of values or vectors ordered by time, where each time step is referred to as a *point*. In anomaly detection tasks, the focus is often placed on contiguous segments of abnormal

behaviors, termed as *anomalous events*. Accordingly, the goal of *Time Series Anomaly Detection (TSAD)* is to identify these anomalous events and their corresponding anomalous points.

A large body of literature has proposed various detection approaches, ranging from statistical models to deep learning frameworks [13]–[23]. However, this work focuses not on the detection algorithms themselves, but rather on how to *evaluate* the effectiveness of their detection results.

In a typical TSAD task, a detector outputs a sequence of continuous anomaly scores:

$$s = [s_1, s_2, \dots, s_T],$$

where  $s_t$  denotes the confidence or probability that the time point t is anomalous. The core objective of evaluation is to map this score sequence into an overall performance score, so as to compare the relative quality of different detectors.

- 2) Evaluation Procedure and Computation Rules: The evaluation process generally consists of three consecutive stages, as illustrated in Fig. 2:
  - Score Generation: The detector outputs an anomaly score for each time point, indicating its likelihood of being anomalous.
  - Thresholding: A threshold  $\tau$  is applied to convert the continuous score sequence into binary predictions,  $\hat{y}_t = I(s_t > \tau)$ . The threshold may be determined by a fixed rule, such as mean+n-std, or by adaptive approaches, e.g., the non-parametric dynamic threshold proposed in [24].
  - Performance Evaluation: Once binary predictions are obtained, evaluation reduces to measuring the consistency between the detected results and the ground truth (GT) labels.

Let both the predicted results and the ground-truth labels be represented as binary time sequences, either on a point-wise, segment-wise, or sequence-wise basis. The standard definitions are as follows:

TP: Correctly detected anomalous points or segments,

FP: Normal parts incorrectly marked as anomalies,

FN: Undetected anomalies,

TN: Normal parts correctly identified as non-anomalous.

Based on these definitions, *Precision*, *Recall*, and *F-measure* are defined as:

$$P = \frac{TP}{TP + FP}, \quad R = \frac{TP}{TP + FN}, \quad F_{\beta} = (1+\beta^2)\frac{P \cdot R}{\beta^2 P + R},$$

where  $\beta=1$  is commonly used to balance precision and recall. The ground-truth anomaly labels may be represented in several forms:

- **Pointwise:** The ground truth is represented as a list of discrete time points that are labeled as anomalous. Each timestamp t is individually marked as normal (0) or abnormal (1), forming a sparse set of 'anomalous points'. This representation is commonly used when anomalies occur instantaneously, such as spikes or sensor glitches.
- **Segmentwise:** The ground truth is given as a collection of time intervals [start, end], each describing a continuous period during which the system is considered to be in

an abnormal state. This form emphasizes the \*temporal continuity\* of anomalies—reflecting the fact that once a fault or deviation starts, it usually persists for several time steps. Segmentwise ground truths are widely adopted in benchmarks that evaluate event-level detection, where detecting any part of an abnormal segment is considered a valid response.

• Sequencewise: The ground truth is encoded as a binary array of length T, where each element indicates whether the corresponding time step belongs to an anomaly (1) or not (0). This representation provides a unified form that can express both pointwise and segmentwise anomalies, enabling algorithmic processing.

It is worth noting that GT labels in practical scenarios are often *imprecise*. The start and end boundaries of anomalous events can be ambiguous, and inter-annotator disagreements may lead to inconsistent GT annotations. Such label uncertainty can introduce substantial bias into evaluation results, thereby complicating interpretation and comparison across studies.

- 3) Thresholding and Definition of Binary Evaluation Metrics: Thresholding serves as a critical dividing step in the evaluation pipeline:
  - Metrics computed after thresholding are termed Binary Metrics. It evaluate the combined effect of the detector and its thresholding strategy. They are based on the confusion matrix (TP, FP, FN, TN) and include classical measures such as Precision, Recall, and their harmonic combination, the F1-score;
  - Metrics computed directly from raw scores are termed Non-binary Metrics. In contrast, it bypasses the thresholding step and operates directly on the continuous anomaly scores. Representative examples include AUC, VUS, and P@K. These metrics assess the detector's global discriminative ability through ranking or integral measures over all thresholds, thereby providing a threshold-independent comparison across detectors.

In general, binary metrics emphasize operational effectiveness in deployment, while non-binary metrics focus on intrinsic discriminative capability at the model level. Balancing these two perspectives remains one of the core challenges in establishing a fair and meaningful evaluation system for time series anomaly detection.

# B. Existing Classification Methods for Evaluation Metrics and Their Limitations

Existing literature commonly classifies evaluation metrics based on their *definition form* and *computational characteristics*.

Traditional surveys [25] adopt a *form-based* taxonomy, where metrics are first divided into two broad groups — **binary** and **non-binary** evaluation metrics — depending on whether a thresholding step is involved.

Binary evaluation metrics compute performance from thresholded predictions and are typically organized into families of precision/recall-based measures. They include classical point-wise F-scores, adjusted point-wise variants and redefined event-level metrics that account for temporal continuity or tolerance. In addition to this, other binary metrics, such as TD and NAB, incorporate time-delay penalties or window-based reward functions.

Non-binary evaluation metrics instead operate directly on the continuous anomaly scores, thereby avoiding the need for an explicit threshold. This group covers single-threshold ranking metrics and integral-based metrics that evaluate performance across all possible thresholds.

TABLE I
TABLE OF ABBREVIATIONS AND FULL NAMES OF VARIOUS METRICS

Abbreviations	Full Names
$PwF_{\beta}$	Point-wise F-score [26]–[29]
$PAF_{\beta}$	Point Adjusted F-score [30]
$SF_{\beta}$	Segment-wise F-score [24]
$CF_{\beta}$	Composite F-score [31]
$dT$ - $PAF_{\beta}^{k}$	Delayed threshold Point Adjusted F-score [32]
NAB	NAB Score [33]
$RF^{\alpha}_{\beta}$	Range-based F-score [34]
$TF^{\tau}_{\beta}$	Time tolerant F-score [35]
TD	Temporal distance [36]
$AF_{eta}$	Affiliation-based F-score [37]
$TaF^{\delta}_{\beta}$	Time series aware F-score [38]
$eTaF_{eta}$	Enhanced time series aware F-score [39]
$VUS^l$	Volume Under Surface [40]
$PATE^{\varepsilon\delta}$	Proximity-Aware Time series Evaluation [41]
$LSF^w$	Latency and Sparsity-aware F-score [29]
P@K	Precision at K [40], [42]
$K\%$ - $PAF_{\beta}^{k}$	K%-Point-adjusted F-score [43]
Best- $PwF$	Best Threshold Binary Metrics [44]
AUC	Area Under Curve [4], [45]–[50]

From a practical standpoint, the above classification emphasizes the *computational form* rather than the *functional purpose* of metrics. However, in real-world applications, practitioners are often more concerned with what problem a metric can solve and how the evaluation outcome maps to operational or experimental needs. Therefore, this work adopts a *problemoriented* classification perspective: starting from the criteria of comparability and fairness, and then categorizing metrics by their functional roles in application contexts. As shown in Fig. 1, the framework consists of two complementary dimensions(for the meanings of abbreviations, please refer to Table I):

# Comparability & Robustness Dimension (Foundational):

- Threshold-dependence / Parameter-free: Indicates
  whether the metric relies on user-defined or data-driven
  hyperparameters (e.g., thresholds, window sizes). In
  cross-model benchmarking, threshold-dependent metrics
  often hinder fair comparison, whereas parameter-free
  metrics (e.g., AUC, AP) are more suitable for objective
  evaluation.
- Label-robustness: Measures the stability of the metric under uncertain or inconsistent ground-truth boundaries.
   In industrial anomaly detection where human labeling errors or vague event boundaries are common, this property is crucial for reliable evaluation.

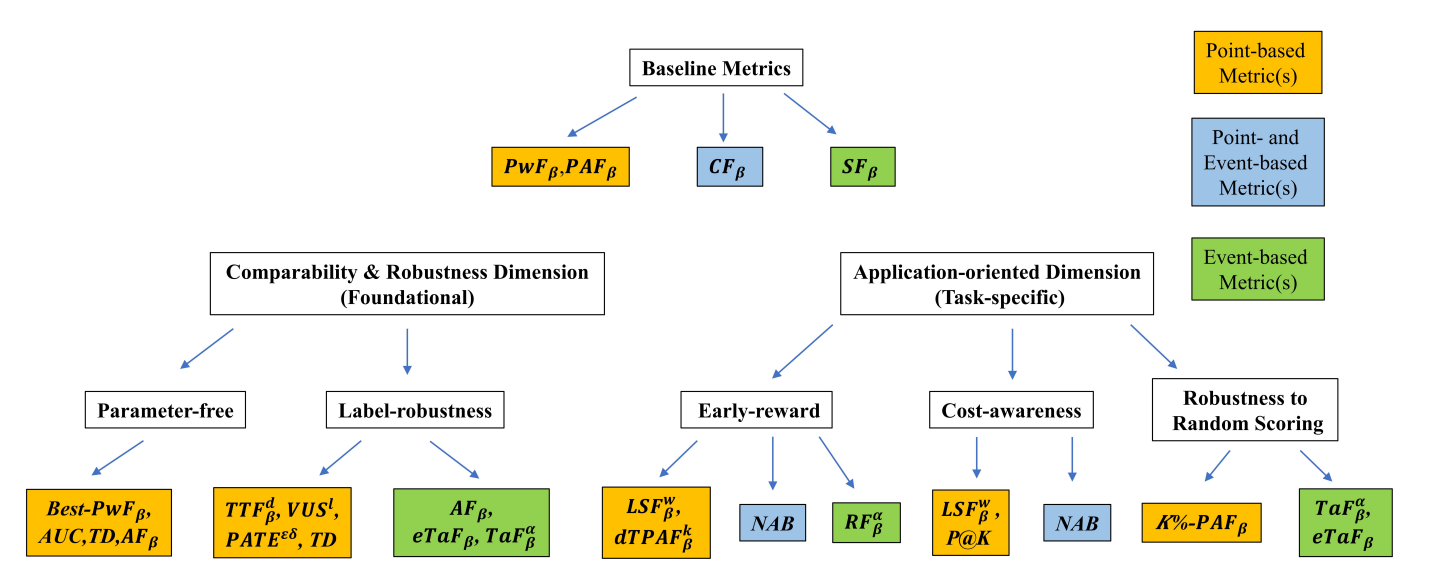


Fig. 1. Problem-oriented Taxonomy of Time Series Anomaly Detection Metrics. This figure illustrates the proposed problem-oriented taxonomy of anomaly detection metrics. The framework is organized along two principal dimensions: a Foundational dimension emphasizing comparability and robustness (e.g., parameter-free and label-robust metrics), and an Application-oriented dimension reflecting task-specific evaluation goals (e.g., early-reward, cost-awareness, and robustness to random scoring). Each subcategory is associated with representative metrics, color-coded by their granularity — point-based (yellow), event-based (green), or hybrid (blue). This hierarchical structure highlights how different metrics are designed to address distinct evaluation challenges and reveals their conceptual interrelations.

# **Application-oriented Dimension (Task-specific):**

- **Timeliness / Early-reward:** Evaluates whether the metric provides additional rewards for early detection. In domains such as fault prediction or financial risk control, metrics incorporating temporal weighting better reflect practical requirements.
- Cost-awareness / Sparse-alarm penalty: Assesses whether the metric accounts for the operational cost of false alarms or human verification. In high-cost settings (e.g., industrial monitoring, medical diagnosis), cost-weighted metrics align more closely with real-world utility.
- Score-stability / Robustness to random scoring: Examines whether the metric design inherently suppresses artificially inflated scores from random or sparse predictions. This property is critical in adversarial or noisy environments, ensuring that speculative or trivial alerting strategies do not appear deceptively effective.

This problem-oriented classification does not restrict a metric to a single category. Instead, it provides researchers and engineers with a diagnostic toolkit: first assess the metric's comparability and robustness properties, then select or design appropriate metrics based on task demands (e.g., timeliness, cost sensitivity). For practical usability, later sections will present a tabular mapping between common evaluation metrics and the above dimensions, followed by case studies illustrating how metric selection can affect evaluation conclusions. Such a framework highlights the practical relevance and task adaptability of metrics, offering a systematic perspective for metric selection and design in diverse TSAD applications.

## III. DETAILED METRICS

#### A. Baseline Metrics

1) Point-wise Metrics:

## a) Point-wise F-score ( $PwF_{\beta}$ ):

A basic evaluation paradigm treats every timestamp in a time series as an independent classification instance, i.e., deciding whether the point at time t is anomalous. From this viewpoint, the point-wise F-score  $(PwF_{\beta})$  naturally follows. Its core idea is to compare ground-truth labels and model predictions on a per-time-step basis, count true positives, false positives and false negatives, and then compute Precision, Recall and the F-score in the standard way. Under this metric a prediction is considered correct only if it coincides exactly with the ground-truth label at the same time step; hence, the metric emphasizes temporal localization accuracy and is suitable for applications that require strict timestamp-level detection (e.g., system security monitoring or financial fraud detection).

The advantages of point-wise metrics are simplicity, interpretability, and direct computability, which explains their widespread usage in early TSAD research [26]–[29]. However, they are overly punitive for small boundary shifts, so a detection that approximately captures an anomalous interval may still obtain a low score. Consequently, point-wise metrics may underestimate practical detection effectiveness when ground-truth boundaries are fuzzy or noisy.

Formally, let the time series length be T, the ground-truth label at time t be  $y_t \in \{0,1\}$  and the predicted binary label be  $\hat{y}_t \in \{0,1\}$ . Define

$$TP = \sum_{t=1}^{T} y_t \hat{y}_t, \quad FP = \sum_{t=1}^{T} (1 - y_t) \hat{y}_t, \quad FN = \sum_{t=1}^{T} y_t (1 - \hat{y}_t).$$

Precision, Recall and  $F_{\beta}$  are then computed in the usual way:

$$P = \frac{\mathrm{TP}}{\mathrm{TP} + \mathrm{FP}}, \quad R = \frac{\mathrm{TP}}{\mathrm{TP} + \mathrm{FN}}, \quad F_{\beta} = (1 + \beta^2) \frac{P \cdot R}{\beta^2 P + R}.$$

b) Point Adjusted F-score ( $PAF_{\beta}$ ):

To mitigate the excessive strictness of point-wise metrics,

the *point-adjusted* approach was proposed [30]. The basic idea is simple and application-driven: if a model predicts at least one positive point within a ground-truth anomalous interval, that entire interval is considered "detected". This reflects the practical logic that, in many scenarios, a single alert is sufficient to trigger a human investigation.

Concretely, let the set of ground-truth anomalous segments be

$$\mathcal{G} = \{ [s_i, e_i] \}_{i=1}^{N_g},$$

and let the original binary predictions be  $\{\hat{y}_t\}_{t=1}^T$ . The point-adjusted prediction  $\tilde{y}_t$  is obtained by adjusting predictions within each ground-truth segment as follows:

$$\tilde{y}_t = \begin{cases} 1, & \text{if } \exists i \text{ s.t. } t \in [s_i, e_i] \text{ and} \\ \exists u \in [s_i, e_i] \text{ with } \hat{y}_u = 1, \\ \hat{y}_t, & \text{otherwise.} \end{cases}$$

In words: for any ground-truth segment that contains at least one predicted positive, mark all points inside that ground-truth segment as positive in the adjusted prediction. After forming  $\tilde{y}_t$ , compute TP, FP and FN using  $\tilde{y}_t$  in place of  $\hat{y}_t$ , and then obtain Precision/Recall/ $F_\beta$  as usual.

Point-adjusted metrics substantially relax the full-coverage requirement and are well-suited to long anomaly intervals (e.g., equipment failures where an early alarm suffices). Their shortcoming is that they can be overly generous: a model that outputs overly long predicted anomalous segments (or random long predictions) can achieve high PA scores. For this reason, PA metrics are often used together with additional precision constraints or complementary measures.

#### 2) Event-level Metrics:

# a) Segment-wise F-score $(SF_{\beta})$ :

Segment-wise evaluation treats each continuous anomalous interval as an individual event, and counts whether each event is detected or missed [24]. Let the ground-truth segments be

$$\mathcal{G} = \{G_i = [s_i, e_i]\}_{i=1}^{N_g},$$

and the predicted segments be

$$\mathcal{P} = \{P_j = [s'_j, e'_j]\}_{j=1}^{N_p}.$$

Define the overlap predicate between two intervals as

overlap(
$$[s_1, e_1], [s_2, e_2]$$
): =  $\neg (e_1 < s_2 \lor e_2 < s_1)$ ,

equivalently  $s_1 \leq e_2$  and  $s_2 \leq e_1$ .

The confusion counts for segment-level evaluation are then:

$$\begin{aligned} &\operatorname{TP}_{\operatorname{seg}} = \left| \left\{ G_i \in \mathcal{G} \mid \exists P_j \in \mathcal{P}, \ \operatorname{overlap}(G_i, P_j) \right\} \right|, \\ &\operatorname{FN}_{\operatorname{seg}} = \left| \left\{ G_i \in \mathcal{G} \mid \forall P_j \in \mathcal{P}, \ \neg \operatorname{overlap}(G_i, P_j) \right\} \right|, \\ &\operatorname{FP}_{\operatorname{seg}} = \left| \left\{ P_j \in \mathcal{P} \mid \forall G_i \in \mathcal{G}, \ \neg \operatorname{overlap}(P_j, G_i) \right\} \right|. \end{aligned}$$

Precision and Recall at the event (segment) level are

$$P_{\text{seg}} = \frac{\text{TP}_{\text{seg}}}{\text{TP}_{\text{seg}} + \text{FP}_{\text{seg}}}, \qquad R_{\text{seg}} = \frac{\text{TP}_{\text{seg}}}{\text{TP}_{\text{seg}} + \text{FN}_{\text{seg}}},$$

and the Segment-wise  $F_{\beta}$  is computed as

$$SF_{\beta} = (1 + \beta^2) \frac{P_{\text{seg}} \cdot R_{\text{seg}}}{\beta^2 P_{\text{seg}} + R_{\text{seg}}}.$$

Segment-wise metrics focus on whether events are detected at least once, thus avoiding the long-segment bias of pointwise counts and aligning well with many expert needs. Their drawbacks include insensitivity to predicted segment length (a very long predicted interval that overlaps with a single ground-truth event is not penalized) and a limited reflection of false alarms within non-overlapping normal regions. Consequently, they can be gamed by coarse, high-coverage predictions and may over-estimate practical utility if used alone.

# 3) Composite Metrics:

# *a)* Composite F-score ( $CF_{\beta}$ ):

Event-level metrics and point-wise metrics are complementary: the former emphasize event discovery (recall at event level) while the latter emphasize localization precision. To balance these two perspectives, the *composite F-score* ( $CF_{\beta}$ ) integrates an event-level recall with a point-wise precision via a harmonic combination [31].

Specifically, let event-level recall be

$$R_{\text{seg}} = \frac{\text{TP}_{\text{seg}}}{\text{TP}_{\text{seg}} + \text{FN}_{\text{seg}}},$$

and point-wise precision be

$$P_{\text{point}} = \frac{\text{TP}_{\text{point}}}{\text{TP}_{\text{point}} + \text{FP}_{\text{point}}},$$

where  $\mathrm{TP}_{\mathrm{point}}, \mathrm{FP}_{\mathrm{point}}$  are the standard point-wise counts (as defined in the point-wise subsection). The composite F-score is then

$$CF_{\beta} = (1 + \beta^2) \frac{P_{\text{point}} \cdot R_{\text{seg}}}{\beta^2 P_{\text{point}} + R_{\text{seg}}}.$$

This construction penalizes methods that achieve high event recall at the expense of very low point-wise precision, thereby providing a more balanced assessment in event-detection tasks. Note that CF depends on both the event segmentation of the ground truth and the point-wise behavior of predictions, so it can be sensitive when anomaly segment lengths vary widely.

### B. Timeliness and Early Detection Metrics

In many time-critical domains—such as industrial fault prevention, medical monitoring, or financial risk control—the *timeliness* of anomaly detection becomes a key evaluation dimension. Traditional point- or segment-level F-scores only measure whether anomalies are correctly identified but remain insensitive to *when* they are detected. Consequently, they fail to capture the operational value of early alarms, where even a short advance warning can substantially mitigate downstream losses. To address this limitation, a series of *timeliness-aware* metrics have been proposed to explicitly reward earlier detections while penalizing delayed or redundant alerts.

1) Delayed threshold Point Adjusted F-score  $(dT-PAF_{\beta}^k)$ : This metric assumes that if a model raises an alarm within the first k time steps of a true anomaly segment, the anomaly is considered "timely captured." Even if later predictions deviate, the segment is still treated as successfully detected. Conversely, if the detection delay exceeds k, the entire segment is regarded as a miss, thereby penalizing late detections [32].

This better aligns with real-world scenarios where early detection can prevent major losses. However, it may overestimate precision for long anomaly segments.

Such a design highlights the model's responsiveness — in applications where "early discovery" is of paramount importance, it effectively distinguishes models with stronger temporal sensitivity. Meanwhile, by restricting detections to the first k steps, it partially mitigates the impact of random hits in long anomaly segments. Nonetheless, the choice of k remains subjective; the definition of "timely" may vary across domains, limiting cross-task comparability.

**Computation.** Let the true anomaly segment be [s,e]. If there exists any predicted point  $\hat{y}_t=1$  within the window [s,s+k-1] (where  $s+k-1\leq e$ ), the entire segment is marked as detected:

$$y_t = 1, \quad \forall t \in [s, e].$$

Otherwise, all predicted points within this segment are removed and counted as false negatives (FN). After this adjustment, the point-wise counts TP, FP, FN are recalculated, and the score is defined as:

$$dT - PAF_{\beta}^{k} = \frac{(1+\beta^{2}) \cdot TP}{(1+\beta^{2}) \cdot TP + \beta^{2} \cdot FN + FP},$$

where  $\beta$  controls the trade-off between precision and recall.

#### 2) NAB Score:

To address the same timeliness requirement, Numenta proposed the *Numenta Anomaly Benchmark (NAB) Score*, a widely recognized framework that integrates *detection accuracy*, *timeliness*, and *false alarm sparsity* [33].

The NAB design revolves around *temporal windows* and *dynamic weighting*. For each true anomaly segment, a detection window of equal length is defined. If a prediction falls within this window, it receives a reward based on its position — earlier detections are rewarded more, while delayed detections are penalized.

Specifically, the reward function is modeled by a scaled sigmoid:

$$S(r) = \begin{cases} -1, & r > 3.0, \\ 2 \cdot \text{sigmoid}(-5r) - 1, & \text{otherwise,} \end{cases}$$

where:

- For detections **inside** the window:  $r = -\frac{R_i t + 1}{W}$ , with  $R_i$  the right boundary of the window, t the detection time, and W the window width.
- For **false alarms** outside the window:  $r = \frac{|t R_{\text{prev}}|}{W_{\text{prev}} 1}$ , where  $R_{\text{prev}}$  and  $W_{\text{prev}}$  denote the boundary and width of the nearest preceding window.

Each window contributes at most one positive reward (the maximum within-window score). False alarms accumulate negative scores:

$$RawScore = \sum_{i} \max_{t \in W_i} (w_{tp} \cdot S(r_t)) - \sum_{j} w_{fp} \cdot S(r_j),$$

where  $w_{tp}$  and  $w_{fp}$  are weighting factors for true and false detections.

The final NAB score is normalized as:

$$\label{eq:NAB} {\rm NAB} = 100 \cdot \frac{{\rm RawScore} - {\rm NullScore}}{{\rm PerfectScore} - {\rm NullScore}},$$

where *NullScore* represents the baseline (no detections) and *PerfectScore* corresponds to ideal performance.

# 3) Range-based F-score $(RF^{\alpha}_{\beta})$ :

In complex real-world scenarios, binary hit/miss outcomes — even at segment-level — often fail to fully capture detection quality. Different tasks prioritize different goals: some emphasize *early detection*, others *comprehensive coverage*, and others wish to avoid *redundant detections*. To unify these perspectives, researchers proposed the **Range-based F-score**  $(RF^{\alpha,\beta})$ , a flexible metric framework that integrates various reward and penalty mechanisms through customizable functional modules [34].

The key idea is to decompose traditional *precision* and *recall* into modular components:

- Existence function determines whether a true or predicted interval is hit at least once;
- 2) **Coverage function** quantifies the degree of overlap;
- 3) **Cardinality function** penalizes multiple detections of the same true interval;
- 4) **Positional function** weights detections based on temporal preferences (e.g., early vs. late).

By tuning these modules and their parameters, the metric can adapt to diverse application objectives. For instance, in security monitoring, the positional function can emphasize "earlier is better," while in industrial quality control, the coverage term can dominate to ensure *complete detection*. This modularity grants  $RF^{\alpha,\beta}$  high interpretability and task adaptability.

However, the cardinality penalty g(n) (often g(n) = 1/n) can introduce excessive subjectivity. Its original intent is to prevent *artificial inflation* — e.g., splitting one true anomaly into many small predictions to boost recall — but it may overly penalize slightly fragmented yet legitimate detections.

For example, when a model produces multiple short but adjacent detections for the same anomaly, the overall coverage may still be sufficient, yet the score is forcibly compressed by 1/n. This bias favors *compact* detections, which is suitable for single-alarm settings but distorts evaluation for continuous monitoring or multi-level alert systems. Hence, careful tuning of the penalty and positional functions is recommended.

**Computation.** Let  $I_r$  and  $I_p$  denote the sets of true and predicted anomaly intervals. For any  $i \in I_r, j \in I_p$ , let overlap(i,j) denote their intersection length and |i| the length of interval i.

#### Existence

$$\begin{split} E_i^r &= \mathbb{I}\{\exists j \in I_p : \text{overlap}(i,j) > 0\}, \\ E_j^p &= \mathbb{I}\{\exists i \in I_r : \text{overlap}(i,j) > 0\}. \end{split}$$

## Coverage

$$\mathrm{cov}(i) = \frac{\sum_{j} \mathrm{overlap}(i,j)}{|i|}, \quad C_i^r = \mathrm{Transform}(\mathrm{cov}(i)),$$

where *Transform* can be identity, truncation, or another monotonic function.

## • Positional Weight

$$\omega_{ij}^r \in [0,1],$$

representing the relative importance of overlap location within i, controlled by shape parameters such as flat, early, or late. Normalized forms satisfy  $\sum_{i} \omega_{ij}^{r} = 1$ .

# · Cardinality Penalty

$$n_i = |\{j \in I_p : \text{overlap}(i, j) > 0\}|,$$

 $g(n_i)$  is a non-increasing function (e.g., g(n) = 1 or 1/n).

Then, the weighted contribution of each true interval is:

$$S_i^r = \alpha \cdot E_i^r + (1 - \alpha) \cdot g(n_i) \cdot \sum_j \omega_{ij}^r.$$

The recall and precision are computed as:

$$R^{\alpha} = \frac{1}{|I_r|} \sum_{i \in I_r} S_i^r, \quad P^{\alpha} = \frac{1}{|I_p|} \sum_{j \in I_p} S_j^p.$$

Finally, the overall range-based F-score is given by:

$$RF^{\alpha}_{\beta} = \frac{(1+\beta^2)P^{\alpha}R^{\alpha}}{\beta^2P^{\alpha} + R^{\alpha}}.$$

4) Latency and Sparsity-aware F-score ( $LSF^w$ ):

The  $LSF^w$  metric implements an early-detection reward and late-detection penalty through a *detection state propagation* mechanism. Specifically, when the model successfully detects at least one true anomaly within a window  $W_i$ —that is,

$$\exists t \in W_i : \hat{y}_t = 1 \land y_t = 1,$$

the window enters the *detection-activated state*. In this case, LSF propagates the detection state from the first true anomalous point

$$s_i = \min\{t \in W_i : y_t = 1\}$$

to the end of the window, forcing all predictions in this interval to be positive:

$$\hat{y}_t^* = 1$$
,  $\forall t \in [s_i, \max(W_i)]$ , if  $\exists \tau \in W_i : \hat{y}_\tau = 1 \land y_\tau = 1$ .

This design embodies two layers of evaluation logic:

- 1. **Reward for early detection.** If the model raises an alarm near the beginning of an anomalous segment (i.e., close to  $s_i$ ), all subsequent points inherit correct predictions without requiring additional detections. This provides a positive incentive for "fast response"—the earlier the detection, the larger the implicit trust and the higher the recall.
- 2. **Penalty for delayed detection.** Conversely, if the model detects the anomaly only near the end of the window (e.g., close to  $\max(W_i)$ ), all earlier missed points

$$t \in [s_i, \tau), \qquad \tau = \text{first detected point},$$

remain counted as false negatives. Thus, delayed detections cannot obtain full batch-level trust propagation, yielding significantly lower scores than timely detection.

In addition, LSF introduces cross-window persistence of the detection state: once a window becomes detection-activated, the state is propagated into the next window as long as ground-truth anomalies remain continuous (i.e., no  $y_t=0$ 

is encountered). This ensures coherent evaluation of long anomalous segments and avoids artificial penalties caused by window boundaries. However, the detection state is immediately reset when a normal point appears, forcing the model to re-demonstrate its detection capability at the beginning of each new anomalous segment, thereby maintaining evaluation strictness.

**Computation.** Given a window size  $w \in \mathbb{Z}^+$ , the calculation proceeds as follows:

The first step is window partition. The sequence is divided into batches:

$$W_i = [iw + 1, \min((i+1)w, T)],$$
  
 $i = 0, 1, \dots, B - 1, \quad B = \lceil T/w \rceil.$ 

And the next step is delay adjustment. For each window  $W_i$ , define the first anomaly as:

$$s_i = \begin{cases} \min\{t \in W_i : y_t = 1\}, otherwise, \\ \infty, \text{ if no anomaly exists.} \end{cases}$$

Define a detection-state flag  $DS_i \in \{0,1\}$  updated by:

$$\mathrm{DS}_i = \begin{cases} &\text{if } \exists \, t \in W_i : \hat{y}_t = 1 \land y_t = 1\\ 1, & \land \; (\mathrm{DS}_{i-1} = 1 \ \lor \ t = s_i),\\ 0, &\text{if } \forall \, t \in W_i : y_t = 0. \end{cases}$$

The adjusted prediction sequence is:

$$\hat{y}_t^* = \begin{cases} 1, & t \in [s_i, \max(W_i)] \land \mathrm{DS}_i = 1, \\ \hat{y}_t, & \text{otherwise.} \end{cases}$$

The batch-adjusted ground-truth labels are:

$$y_t^* = \begin{cases} 1, & t \in [s_i, \max(W_i)], \\ 0, & \text{otherwise.} \end{cases}$$

For each window, batch-level Confusion Matrix:

$$TP_{i} = \mathbb{I} [\exists t \in W_{i} : y_{t}^{*} = 1 \land \hat{y}_{t}^{*} = 1],$$
  

$$FP_{i} = \mathbb{I} [\exists t \in W_{i} : y_{t}^{*} = 0 \land \hat{y}_{t}^{*} = 1],$$
  

$$FN_{i} = \mathbb{I} [\exists t \in W_{i} : y_{t}^{*} = 1 \land \hat{y}_{t}^{*} = 0],$$

where  $\mathbb{I}[\cdot]$  denotes the indicator function.

Global aggregation and metric computation:

$$\begin{aligned} \text{TP} &= \sum_{i=0}^{B-1} \text{TP}_i, \quad \text{FP} &= \sum_{i=0}^{B-1} \text{FP}_i, \quad \text{FN} &= \sum_{i=0}^{B-1} \text{FN}_i. \\ LSF^w &= \frac{2\text{TP}}{2\text{TP} + \text{FP} + \text{FN}}. \end{aligned}$$

# C. Label-robust Metrics (Mitigating Annotation Uncertainty)

In real-world applications, anomaly annotations often contain uncertainties. The start or end boundaries of anomalies may slightly deviate from their actual occurrence time due to human judgment or noise contamination. Consequently, traditional point-wise metrics can suffer severe score degradation caused by minor temporal misalignment, leading to an unfair evaluation of detection ability. To address this, several label-robust metrics have been proposed to tolerate annotation uncertainty and boundary fuzziness.

# 1) Time tolerant F-score $(TF_{\beta}^{\tau})$ :

The core idea of the time-tolerant F-score is to introduce a temporal tolerance radius d, such that a prediction is considered correct as long as it occurs within d time steps of a true anomaly [35]. This mechanism mitigates harsh penalties for slightly advanced or delayed detections, providing a more realistic reflection of system performance in practice. It is especially effective for short anomaly segments, where single-point misalignment could otherwise cause disproportionate score drops.

**Computation.** For each predicted anomaly point  $\widehat{y_t} = 1$ , if there exists a true anomaly point a satisfying  $|t - a| \leq d$ , it is counted as a true positive. The time-tolerant precision and recall are defined as:

$$R_d = \frac{1}{|E|} \sum_{t: y_t = 1} \mathbb{I}\left(\sum_{j=t-d}^{t+d} \widehat{y_j} = 1\right),$$

$$P_d = rac{1}{|A|} \sum_{t:\widehat{y}_t=1} \mathbb{I}\left(\sum_{j=t-d}^{t+d} y_j = 1\right)$$

where d is the tolerance radius, E the set of true anomalies, and A the set of predicted anomalies. Then the time-tolerant F-score is given by:

$$TF_{\beta}^d = \frac{(1+\beta^2)P_dR_d}{\beta^2 P_d + R_d}.$$

# 2) Temporal distance (TD):

To further quantify the temporal offset between predicted and true anomalies, the *Temporal distance (TD)* metric adopts a bidirectional nearest-neighbor distance strategy [36]. For each true anomaly, the minimum temporal distance to any predicted point is computed, and vice versa. The final TD score sums both distances, measuring the localization accuracy along the time axis—smaller TD values indicate better temporal precision.

**Computation.** Let  $A = \{s : y_s = 1\}$  and  $B = \{t : \widehat{y_t} = 1\}$  denote the sets of true and predicted anomaly points, and L the sequence length. Then:

$$TD = \sum_{s \in A} d(s, B) + \sum_{t \in B} d(t, A), \tag{1}$$

where

$$d(s,B) = \begin{cases} \min_{t \in B} |s-t|, & \text{if } B \neq \emptyset, \\ L, & \text{if } B = \emptyset, \end{cases}$$

$$d(t,A) = \begin{cases} \min_{s \in A} |t-s|, & \text{if } A \neq \emptyset, \\ L, & \text{if } A = \emptyset. \end{cases}$$

This design ensures consistent penalization and robustness even when either the prediction or ground truth is empty.

# *3)* Affiliation-based F-score $(AF_{\beta})$ :

The affiliation-based F-score alleviates label uncertainty by quantifying the distance-based closeness between predicted and true anomalies [37]. Instead of requiring strict overlap, it transforms temporal proximity into a probabilistic affinity score, offering interpretability and robustness against boundary fuzziness.

**Computation.** The computation involves three steps. First, for each true anomaly segment  $\mathcal{J} = \{J_1, \ldots, J_m\}$ , define its corresponding membership region:

$$E_i = \left(\frac{t_{\text{stop}}^{i-1} + t_{\text{start}}^i}{2}, \frac{t_{\text{stop}}^i + t_{\text{start}}^{i+1}}{2}\right).$$

Next, project each predicted segment  $I \in \mathcal{I} = \{I_1, \dots, I_n\}$  onto the associated membership region:

$$\mathcal{P}_i = \{ I \cap E_i : I \in \mathcal{I}, I \cap E_i \neq \emptyset \}.$$

Then, compute the Affiliation-based precision and recall within each region via integration:

$$P_{AF} = \frac{\sum_{i=1}^{m} \sum_{I \in \mathcal{P}_i} \int_{I} p_{\text{precision}}(x, J_i, E_i) dx}{\sum_{I \in \mathcal{I}} |I|},$$

$$R_{AF} = \frac{\sum_{i=1}^{m} \int_{J_i} p_{\text{recall}}(x, \mathcal{P}_i, E_i) dx}{\sum_{i=1}^{m} |J_i|}.$$

Finally, aggregate them using:

$$AF_{\beta} = (1+\beta^2) \frac{P_{AF}R_{AF}}{\beta^2 P_{AF} + R_{AF}}.$$

# 4) Time series aware F-score $(TaF_{\beta}^{\delta})$ :

The time series aware F-score introduces both a coverage threshold and a fuzzy tolerance zone to balance temporal robustness and realistic event coverage. It decomposes the detection performance into two dimensions: *detection accuracy* (event-level recognition) and *positional accuracy* (temporal alignment) [38].

Computation. Let the recall and precision be defined as:

$$R = \alpha R_{\text{detection}} + (1 - \alpha) R_{\text{position}}, \tag{2}$$

$$P = \alpha P_{\text{detection}} + (1 - \alpha) P_{\text{position}}, \tag{3}$$

where  $\alpha \in [0,1]$  balances event-level and positional emphasis. **Detection-level components:** 

$$R_{\text{detection}} = \frac{1}{|A|} \sum_{i=1}^{|A|} \mathbb{I}\left(\frac{S_i}{L_i} \ge \theta\right), \tag{4}$$

$$P_{\text{detection}} = \frac{1}{|P|} \sum_{j=1}^{|P|} \mathbb{I}\left(\frac{S_j}{L_j} \ge \theta\right), \tag{5}$$

where  $S_i$  is the overlap between true and predicted segments,  $L_i$  is the anomaly duration, and  $\theta$  is the minimum overlap ratio threshold.

# **Positional components:**

$$R_{\text{position}} = \frac{1}{|A|} \sum_{i=1}^{|A|} \min\left(1, \frac{S_i}{L_i}\right),\,$$

$$P_{\text{position}} = \frac{1}{|P|} \sum_{j=1}^{|P|} \min\left(1, \frac{S_j}{L_j}\right).$$

Here,  $S_i = \text{overlap\_score} + \text{decay\_score}$ , with the latter computed using a sigmoid decay function over a fuzzy window of length  $\delta$ .

The position dimension uses  $\min(1, S_i/L_i)$  to map each anomalous segment into a segment-level score within [0,1], thereby enabling event-level evaluation. However, if the scores of individual segments are subsequently aggregated in a point-weighted manner (e.g., by directly summing  $S_i$ ), long anomaly segments tend to dominate the overall score due to their larger number of points. Conversely, if a simple arithmetic mean is taken across all segments, each segment is treated equally, and the importance of longer anomalies is underestimated. Therefore, the single definition  $\min(1, S_i/L_i)$  is insufficient to balance "point-level precision" and "event-level coverage." An explicit weighting or hybrid aggregation scheme is required to achieve a proper trade-off between the two.

- 5) Enhanced time series aware F-score ( $eTaF_{\beta}$ ): The enhanced version  $eTaF_{\beta}$  introduces a length-weighted iterative pruning mechanism to address TaF's potential overrewarding of irrelevant overlaps. This refinement yields stricter and more application-aligned evaluation. However, as it inherits the fuzzy zone of length  $\delta$ , detailed discussion of its improvement on random-score suppression is deferred to Section 3.5.
- 6) Volume Under Surface (VUS<sup>l</sup>-ROC, VUS<sup>l</sup>-PR): Traditional AUC-based metrics rely on binary (0/1) labels, which can be overly rigid when anomaly boundaries are uncertain. The Volume Under Surface (VUS) metric introduces a soft labeling mechanism with tolerance windows, offering a more robust assessment under label noise and boundary ambiguity [40].

**Computation.** For each true anomaly point, a tolerance window of size w is defined, and predictions within this window receive distance-weighted scores:

$$y_t^{(w)} = \max_{i:|i-t| \le w} y_i \cdot f(|i-t|, w),$$

where the decay function f(d, w) is typically:

$$f(d, w) = \begin{cases} 1 - \frac{d}{w}, & \text{if } d \le w, \\ 0, & \text{otherwise.} \end{cases}$$

Integrating the AUC values across different tolerance scales yields:

$$VUS^{l} = \int_{0}^{w_{\text{max}}} AUC^{(w)} dw.$$

While VUS improves label robustness, it sacrifices the parameter-free property of AUC, making inter-study comparison less direct.

7) Proximity-Aware Time series Evaluation  $(PATE^{\varepsilon\delta})$ : The  $PATE^{\varepsilon\delta}$  metric addresses four major limitations of traditional metrics—temporal blindness, binary decisioning, delay insensitivity, and weak practical relevance—by introducing proximity-weighted regions and adaptive buffer zones [41].

Specifically,  $PATE^{\varepsilon\delta}$  defines three semantic regions around each true anomaly segment—pre-buffer, true, and post-buffer—characterized by parameters  $\varepsilon$  (early-detection buffer) and  $\delta$  (delayed-detection buffer). Predictions are weighted according to their temporal proximity to true anomalies, enabling graded evaluation of "near misses" and "early warnings."

**Computation.** For each true anomaly segment  $A_i = [a_i^s, a_i^e]$ :

$$\mathcal{R}_i^{pre} = [\max(0, a_i^s - \varepsilon, \mathcal{R}_{i-1}^{post} + 1), a_i^s - 1], \quad \mathcal{R}_i^{true} = [a_i^s, a_i^e],$$
$$\mathcal{R}_i^{post} = [a_i^e + 1, \min(a_i^e + \delta, a_{i+1}^s - 1, T)].$$

Predictions are then classified as belonging to one of the regions: true detection, pre-buffer, post-buffer, partial miss, or outside.

**Weighted Scoring.** Weights are assigned to predictions according to their distance from the true segment:

$$w_{\text{pre}}(t, A_i) = 1 - \frac{\sum_{k=a_i^s}^{a_i^s} |k - t|}{\sum_{k=a_i^s}^{a_i^s} |k - \max(0, a_i^s - \varepsilon)|},$$

$$\sum_{k=a_i^s}^{a_i^s} |t - k|$$

 $w_{\text{post}}(t, A_i) = 1 - \frac{\sum_{k=a_i^s}^{a_i^e} |t - k|}{\sum_{k=a_i^s}^{a_i^e} |\min(a_i^e + \delta, T) - k|}.$ 

Finally, weighted precision and recall are computed as:

$$\text{Precision} = \frac{W_{TP}}{W_{TP} + W_{FP}}, \quad \text{Recall} = \frac{W_{TP}}{W_{TP} + W_{FN}},$$

where  $W_{TP}$ ,  $W_{FP}$ ,  $W_{FN}$  denote weighted true positives, false positives, and false negatives respectively.

 $PATE^{\varepsilon\delta}$  supports two evaluation modes:

$$PATE^{\varepsilon\delta} = \frac{1}{|\mathcal{B}_{\varepsilon}||\mathcal{B}_{\delta}|} \sum_{(\varepsilon', \delta') \in \mathcal{B}_{\varepsilon} \times \mathcal{B}_{\delta}} AUC - PR(\theta_k),$$

$$\mathrm{PATE}^{\varepsilon\delta} - \mathrm{F1} = \frac{1}{|\mathcal{B}_{\varepsilon}||\mathcal{B}_{\delta}|} \sum_{(\varepsilon', \delta')} \frac{2 \cdot \mathrm{Precision} \cdot \mathrm{Recall}}{\mathrm{Precision} + \mathrm{Recall}}.$$

Although computationally expensive  $(O(K|\mathcal{B}_{\varepsilon}||\mathcal{B}_{\delta}|N_AN_P))$ ,  $PATE^{\varepsilon\delta}$  provides fine-grained, temporally aware evaluation aligned with real-world anomaly detection requirements.

# D. Cost-aware Metrics (Penalizing Human Verification Effort)

In real-world anomaly detection systems, evaluation should reflect not only detection accuracy but also the cost of human verification. From an operational perspective, different types of false alarms impose unequal burdens on analysts. When false positives are densely clustered, multiple alarms can often be verified collectively, leading to relatively low review effort. In contrast, dispersed false positives require repeated manual checks, incurring substantially higher verification costs. This motivates a class of *sparsity-penalizing metrics* that explicitly punish scattered false alarms to better align with real-world operational costs.

Meanwhile, another form of verification cost arises from limited analyst capacity. In many industrial scenarios, human reviewers can only inspect a small number of high-priority alerts due to time or resource constraints. Therefore, rather

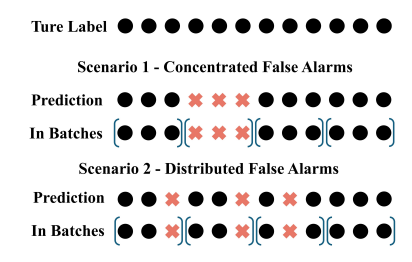


Fig. 2. Concentrated vs. Distributed False Alarms under Batch-level Evaluation. Illustration of how  $LSF^w$  differentiates between concentrated and distributed false alarms. Although both scenarios contain three point-wise false positives, the batch-level penalty differs: only one window is affected in Scenario 1, whereas three windows are affected in Scenario 2. This leads to a higher penalty for distributed false alarms.

than global detection coverage, what matters more is how effectively a model prioritizes true anomalies among its topranked predictions.

# 1) Latency and Sparsity-aware F-score ( $LSF^w$ ):

To reduce the verification cost induced by dispersed false alarms, the latency- and sparsity-aware F-score  $(LSF^w)$  integrates the notion of *false alarm resource cost* into the evaluation process [29].

This metric employs a window-based mechanism that simultaneously models both detection delay and false positive sparsity. For false positive aggregation, LSF adopts a *batchwise* counting scheme: regardless of how many FP points occur within a single time window, they are collectively counted as one FP. This design penalizes dispersed false alarms more heavily than clustered ones, aligning with the real-world observation that scattered false alerts are more disruptive than concentrated bursts.

To illustrate how  $LSF^w$  distinguishes between concentrated and distributed false alarms, consider a time series of length 12 with a window size of w = 3, as shown in fig 2

Under traditional point-wise evaluation, both scenarios yield the same number of false positives (FP=3), and thus receive identical penalties:

Scenario 1: false alarms are concentrated in a local region.
Scenario 2: false alarms are scattered across the timeline.

In contrast,  $LSF^w$  evaluates predictions at the **window** level. For each window  $W_i$ , the batch-level false positive is defined as:

$$\mathrm{FP}_i = \mathbf{1} \bigg[ \max_{t \in W_i} \hat{y}_t = 1 \ \text{and} \ \max_{t \in W_i} y_t = 0 \bigg] \,.$$

This definition implies:If a window contains *any* false positive, the entire window is counted as one batch-level false positive. If a window contains no false positives, it contributes zero.

Therefore, although both scenarios have the same number of point-wise false alarms, their batch-level penalties differ significantly:

**Scenario 1**: only the second window contains false alarms  $\Rightarrow FP_{batch} = 1$ .

**Scenario 2**: three windows contain false alarms  $\Rightarrow$  FP<sub>batch</sub> = 3.

Consequently, distributed false alarms incur a threefold penalty compared to concentrated ones, reflecting their greater operational impact.

#### 2) NAB Score:

The Numenta Anomaly Benchmark (NAB) score extends traditional accuracy metrics by integrating both timeliness and false positive sparsity [33]. For each true anomaly segment, an equal-length detection window is defined. Predictions within this window receive position-dependent rewards: earlier detections yield higher scores, while delayed detections are penalized progressively. False positives outside the window incur distance-based penalties, which increase with their temporal distance from the nearest true anomaly window. Consequently, concentrated false positives are penalized less than dispersed ones.

While NAB reasonably accounts for human verification cost, its penalty strength for FP sparsity is limited. When false positives occur far away (e.g., beyond three times the window length), their penalties quickly saturate near -1. As a result, a cluster of occasional false positives and an equal number of widely scattered ones receive nearly identical penalties—despite vastly different operational impacts. In real-world review scenarios, the former may require only one manual dismissal, whereas the latter could repeatedly interrupt analyst workflows. Hence, NAB's treatment of false positive sparsity remains insufficiently rigorous from a cost perspective.

#### 3) Precision at K (P@K):

In many real-world anomaly detection systems, analysts can only review a limited number of high-priority alerts. Thus, rather than global coverage, what matters more is how effectively a model identifies true anomalies among its topranked predictions. The Precision@K (P@K) metric reflects this concern by evaluating the proportion of true anomalies within the top-K predicted alerts [40], [42].

Specifically, anomaly scores  $s_t$  are sorted in descending order, and the top K predictions are selected as the model's highest-confidence candidates. The proportion of true anomalies within this subset reflects the model's effectiveness under constrained review resources. P@K directly captures the system's alert value density—whether the model provides sufficiently valuable alerts in the most costly review phase.

Compared to global metrics, P@K better aligns with real-world decision processes by emphasizing ranking quality under limited verification budgets. It remains robust even in highly imbalanced datasets, making it an essential measure for evaluating both audit efficiency and operational prioritization. However, since it focuses on only the top-scoring samples, P@K does not comprehensively capture the model's overall detection ability, but rather its prioritization performance under constrained human resources.

**Computation.** Let  $s_t$  denote the anomaly scores and  $y_t$  the ground-truth labels. Then:

$$K = \sum_{t=1}^{T} y_t, \quad \tau = \operatorname{sort}(s_t)_{[-K]},$$
$$\hat{y}_t = \mathbb{I}[s_t \ge \tau],$$

$$P@K = \frac{\sum_{t=1}^{T} \hat{y}_t \cdot y_t}{\sum_{t=1}^{T} \hat{y}_t},$$

where  $\mathbb{I}[\cdot]$  is the indicator function, and  $\operatorname{sort}(s_t)_{[-K]}$  denotes the K-th largest score.

#### E. Robustness to Random or Sparse Scoring

A critical yet often overlooked issue in evaluating time series anomaly detection lies in the vulnerability of certain metrics to random or sparse prediction behaviors. [43] reported that, under specific configurations, random guessing could yield higher scores than state-of-the-art models when using the conventional point-adjusted F1 metric( $PAF_{\beta}$ ). This phenomenon occurs because the metric treats an entire anomalous segment as correctly detected once any single point within it is identified, regardless of the overall detection quality. As a result, sparse or randomly scattered detections may undeservedly achieve inflated scores, undermining the credibility of evaluation results.

To mitigate this, several subsequent studies have introduced mechanisms that explicitly resist random or overly sparse scoring—for example, by imposing temporal consistency requirements or rewarding detection coverage rather than isolated hits. Nevertheless, not all robustness stems from explicit design: some metrics inherently resist random scoring due to their point-based nature, which evaluates detections at a finer temporal granularity.

In this section, we review representative metrics that enhance robustness against random or sparse predictions, followed by a systematic empirical analysis in Section IV to identify which metrics fail to distinguish genuine detector outputs from random or uninformed predictions.

# 1) Time series aware F-score ( $TaF_{\beta}^{\delta}$ ):

 $TaF_{\beta}^{\delta}$  [38] introduces a *coverage threshold* to ensure that model predictions have substantive temporal overlap with true anomaly segments, thereby mitigating artificially high scores caused by random or sparse predictions. As shown in Eq. 4, the computation is performed at the *event level*. The coverage threshold  $\theta$  requires that a prediction must cover at least a certain fraction of a true anomaly segment to be considered a successful detection; otherwise, the entire segment is treated as a miss. This prevents models from achieving inflated scores merely through "spot hits".

#### 2) Enhanced time series aware F-score ( $eTaF_{\beta}$ ):

As noted by Hwang et al. [39], although TaF alleviates the inflation caused by random hits, it may still reward "overlapping but meaningless" detections, where low-quality predictions can still contribute substantial scores. Moreover, TaF lacks a proper length-weighting mechanism, which causes inconsistencies between event- and point-level contributions. To address these limitations, the *Enhanced time series aware F-score* ( $eTaF_{\beta}$ ) introduces an *iterative pruning mechanism* and *length-weighted scoring*, making the evaluation stricter and more realistic.

The core principle of eTaF is that a valid detection must not only overlap sufficiently with the true anomaly segment but also avoid excessive overextension or under-coverage. In implementation, eTaF first constructs an overlap matrix between true and predicted segments, then performs iterative pruning to remove low-quality matches: true segments with recall below  $\theta_r$  and predicted segments with precision below  $\theta_p$  are discarded. This process is repeated until convergence.

After pruning, the retained segments are evaluated by combining detection judgment, overlap ratio, and length-weighted contribution. For instance, each predicted segment is weighted by the square root of its length to prevent disproportionately large contributions from long segments. The resulting eTaR and eTaP represent the recall and precision components, respectively:

eTaR = 
$$\frac{1}{2|A|} \sum_{i=1}^{|A|} (d_i + d_i p_i)$$
, eTaP =  $\frac{1}{2W} \sum_{i=1}^{|P|} \sqrt{L_j} (d_j + d_j p_j)$ ,

where  $d_i$  denotes the detection score,  $p_i$  the localization score, and W the normalization constant. The thresholds  $\theta_r$  and  $\theta_p$  define the minimum acceptable recall and precision levels, while  $\delta$  controls the fuzzy boundary proportion.

Compared to TaF, eTaF offers several advantages: (1) the pruning mechanism effectively filters out low-quality matches, reducing inflated results; (2) the dual-threshold constraints guarantee minimal performance standards for both recall and precision; and (3) length weighting better balances the influence of segments of varying durations. However, this strictness comes at a cost—iterative pruning may remove numerous matches, and tuning  $\theta_r$  and  $\theta_p$  requires task-specific calibration. Furthermore, eTaF incurs higher computational complexity than basic metrics.

# 3) K%-Point-adjusted F-score (K%-PAF<sub>B</sub><sup>k</sup>):

In some anomaly detection tasks, the key concern is not merely whether an anomaly is detected, but whether the detected segment sufficiently *covers* the anomalous process. For instance, in medical monitoring or intrusion detection, isolated and short-lived alarms often lack explanatory value, whereas sustained detections are far more informative. To capture this intuition, the K%-Point-adjusted F-score  $(K\%-PAF_\beta)$  enforces a minimum coverage constraint: only if a predicted segment covers at least K% of the true anomaly points is it considered a successful detection [43]. This constraint prevents models from achieving high scores through accidental or random "flashing" detections.

This coverage-based rule aligns well with human judgment: experts generally consider single-point alerts insufficient, while consistent coverage signals genuine anomaly capture. Thus,  $K\%-PAF_{\beta}$  effectively suppresses inflated scores from random guessing and provides a stricter assessment for long anomaly segments. Nevertheless, its design has tradeoffs—when true anomalies are extremely short or transient, even valid detections may be penalized for insufficient coverage, underestimating practical utility. Moreover, the choice of K is task-dependent and somewhat subjective, limiting cross-scenario comparability.

**Computation.** Let the true anomaly segment be [s,e] with length L=e-s+1. If the number of predicted anomaly

points within this segment satisfies hit  $\geq K \cdot L$ , the entire segment is marked as detected:

$$y_t = 1, \quad \forall t \in [s, e].$$

Otherwise, the predicted points within the segment are removed. The final F-score is then computed based on the adjusted labels:

$$K\%\text{-}PAF_{\beta}^{k} = \frac{(1+\beta^{2})\cdot \mathrm{TP}}{(1+\beta^{2})\cdot \mathrm{TP} + \beta^{2}\cdot \mathrm{FN} + \mathrm{FP}}.$$

## F. Threshold-independent and Parameter-free Metrics

In anomaly detection, continuous anomaly scores must be converted into binary predictions via a threshold to compute conventional classification metrics. However, the selection of such thresholds is often subjective and data-dependent. To mitigate this issue, researchers have proposed using the metric value under the *optimal threshold* as a theoretical upper bound of algorithmic performance, providing a more objective and fair evaluation benchmark. Ignoring the weighting parameter in the F-score, all basic metrics are essentially parameter-free; however, we do not elaborate on them here, as they have already been discussed earlier in the manuscript.

For completeness, we note that the NAB score is a parameterized metric by design, yet all of its hyperparameters have been standardized and fixed in the official specification. Consequently, it requires no additional parameter configuration during use. Since these preset values do not introduce any evaluation mechanisms beyond the scope of this discussion, we do not further elaborate on NAB here.

# 1) Best Threshold Binary Metrics (Best-PwF):

This method exhaustively searches over all possible threshold candidates. For each threshold, a binary classification performance metric (e.g., the  $F_1$  score) is computed, and the maximum value among them is taken as the final evaluation result [44]. Essentially, this approach represents the performance upper limit of a model under *perfect threshold tuning*.

The advantages of this family of metrics are threefold: (1) they provide a theoretical upper bound of algorithmic performance, facilitating potential comparison across different models; (2) they remove the subjectivity of manual threshold selection, ensuring objective and fair evaluation; and (3) they reveal the intrinsic discriminative capacity of the model under ideal conditions. Nevertheless, because this evaluation is idealized, it may not reflect real-world deployment performance. Moreover, the optimal threshold learned from one dataset lacks transferability, potentially leading to biased generalization evaluation.

**Computation.** Let the anomaly score sequence be  $\{s_t\}_{t=1}^T$  and the predicted binary labels be  $\{\hat{y}_t\}_{t=1}^T$ . The  $F_1$  score under the best threshold is defined as:

Best-PwF = 
$$\max_{\theta \in s_t} F_1(\hat{y}_t = \mathbb{I}[s_t \ge \theta])$$
,

where:

- $\theta$  iterates over all unique values in  $\{s_t\}$ ,
- $\mathbb{I}[\cdot]$  is the indicator function,
- $F_1(\cdot)$  is the standard  $F_1$ -score computation function.

## 2) Area Under Curve (AUC-ROC, AUC-PR):

Traditional binary metrics rely on a fixed threshold, which introduces subjectivity and makes optimal threshold selection difficult in practice. To achieve a more comprehensive and objective evaluation, area-under-curve (AUC) metrics assess model performance across all possible thresholds, thereby eliminating the dependence on any single threshold choice [4], [45]–[50].

The key idea behind AUC-based metrics is to quantify a model's overall discriminative ability by integrating performance over varying thresholds. Specifically, *AUC-ROC* (Receiver Operating Characteristic Curve) uses the True Positive Rate (TPR, i.e., recall) as the vertical axis and the False Positive Rate (FPR) as the horizontal axis, capturing the classifier's global discrimination power between positive and negative samples. In contrast, *AUC-PR* (Precision–Recall Curve) plots Precision against Recall, focusing more on the model's ability to detect positive instances. This makes AUC-PR particularly suitable for highly imbalanced anomaly detection tasks.

However, AUC-based metrics also have limitations. For instance, AUC-ROC may yield overly optimistic results in highly imbalanced data due to the large number of true negatives keeping the FPR low. Conversely, AUC-PR is more sensitive to class imbalance but suffers from limited comparability across datasets. Although AUC eliminates threshold dependence during evaluation, in practical deployment, a specific threshold must still be determined to trigger anomaly alarms.

**Computation.** Let  $s_t$  denote the anomaly score and  $y_t$  the ground-truth label. Then:

$$\text{AUC-ROC} = \int_0^1 \text{TPR}(\tau) \, d(\text{FPR}(\tau)),$$

$$\text{AUC-PR} = \int_0^1 \text{Precision}(\tau) \, d(\text{Recall}(\tau)),$$

where  $\tau$  denotes the threshold parameter traversing all possible settings.

From these definitions:

- AUC-ROC is suitable for balanced-class scenarios or when global discrimination capability is of interest.
- AUC-PR is more appropriate for anomaly or rare-event detection tasks, where the positive class is scarce.
- 3) Temporal distance (TD):

TD addresses the issue of annotation uncertainty, but its design is inherently parameter-free, relying entirely on the intrinsic structure of the data rather than any manually specified hyperparameters. As shown in Eq. 1, TD computes a symmetric bidirectional nearest-neighbor distance between predicted and ground-truth anomalous point sets, thereby directly measuring the temporal misalignment between them.

TD reformulates anomaly detection assessment as a point-set matching problem on the time axis, where the evaluation is performed through a deterministic minimum-distance aggregation. The entire procedure contains no tunable components, and every essential element is naturally determined by the input data itself. This design ensures that TD maintains a consistent evaluation standard across datasets and application scenarios, eliminating the potential influence of parameter selection on the evaluation outcome.

## 4) Affiliation-based F-score $(AF_{\beta})$ :

As previously discussed, the integral form of affiliation metrics naturally provides robustness to boundary ambiguity, and its core mechanism is also fully data-driven without relying on any external hyperparameter specification. Excluding the weighting parameter in the F-score, when  $\beta=1$  (i.e., the standard F1 setting), the AF metric becomes a purely data-driven evaluation method that requires no parameter tuning for its application. No manually defined tolerance regions or buffer windows are required. The parameter-free nature of  $AF_{\beta}$  originates from the geometric essence of its "affiliation relation": it partitions the time axis into a set of non-overlapping responsibility regions and evaluates the local prediction fidelity through distance-based integration within each region.

This formulation avoids the binary "perfect match vs. complete mismatch" dilemma present in traditional metrics, replacing it with a continuous probabilistic scoring mechanism that smoothly reflects subtle variations in prediction quality. More importantly, the boundaries of the affiliation regions  $E_i$  are automatically determined by the midpoints between neighboring ground-truth anomalous segments. This automatic region construction guarantees cross-dataset consistency—regardless of the number, length, or spatial distribution of anomalous segments,  $AF_{\beta}$  evaluates predictions under a unified logical framework without requiring parameter adjustments for different scenarios.

#### IV. EXPERIMENTS

This section evaluates the robustness, or "antirandomness" of existing time series anomaly detection metrics when confronted with random or uninformed predictions. All experiments are conducted under strictly controlled and reproducible settings, encompassing a diverse collection of synthetic datasets, various random-prediction strategies, and multiple tiers of detector quality (referred to as the *quality gradient*). Each metric is comprehensively assessed through a suite of statistical indicators to examine the following hypotheses:

- 1) Genuine detectors should yield significantly higher metric scores than random predictions;
- Metrics should demonstrate monotonic consistency along the detection-quality gradient — as detector performance improves (from random to genuine), the corresponding metric scores are expected to increase accordingly.

### A. Datasets and Synthetic Configuration

This experiment systematically evaluates the stability and robustness of different anomaly detection metrics under "uninformative" or "misleading" prediction scenarios. The data generation process follows two principles: *coverage* and *specificity*.

Coverage ensures that the constructed data encompass diverse temporal structures and statistical properties, allowing for a comprehensive examination of metric generality across distributions. Specificity, in contrast, introduces extreme or fragile cases (e.g., isolated anomalies, long-term drifts, periodic perturbations) to assess potential failure risks at distributional boundaries.

It is important to emphasize that this study focuses on the *validation of metrics* rather than the absolute performance of detection models. Therefore, certain scenarios are deliberately designed to yield deceptively high metric scores, thereby revealing possible risks of misleading evaluation in practical applications.

a) Anomaly Types and Generation Mechanisms: The synthetic data include five representative anomaly types to ensure comprehensive coverage across different semantic categories. Their proportions, generation mechanisms, and parameter ranges are summarized below:

- Point anomalies (2.5%) Randomly injected isolated spikes in the sequence, implemented by adding noise with amplitude k · σ<sub>0</sub> (where σ<sub>0</sub> is the baseline standard deviation). These simulate transient faults or sensor glitches, typically lasting 1–3 time steps. The intensity coefficient k is sampled from a predefined parameter range.
- Level shifts (35%) Shifting the signal upward or downward by a constant offset proportional to  $\sigma_0$ . Segment lengths are dynamically assigned to represent short (50–200 points), medium (200–1000 points), and long (> 1000 points) drifts. Two variants are used: additive (mean shift) and multiplicative (amplitude scaling) drift.
- Collective anomalies (25%) Segment-level anomalies involving persistent behavioral changes, including frequency variation, noise amplification, and pattern alteration. Segment lengths range from 10–500 points. Implementation details: (1) Frequency change: replace with a sine wave of a different period; (2) Noise amplification: increase segment noise by a factor of 5; (3) Pattern change: replace with a segment drawn from a distinct statistical distribution.
- **Periodic disruption** (25%) Local disruption of periodic structure, including flattening, phase shifting, and amplitude reduction. Perturbations last between 50–1000 points, primarily used to test the adaptability of metrics in strongly periodic backgrounds.
- Contextual anomalies (12.5%) Locally significant but globally inconspicuous deviations within seasonal or trending contexts. Implemented by temporal context misplacement (replacing with another segment from a different time) or amplitude-context distortion. Segment length ranges from 20–200 points, designed to assess the metric's ability to distinguish local versus global anomalies.

To ensure consistent statistical characteristics, the baseline standard deviation  $\sigma_0$  is computed from the clean signal before anomaly injection. All anomaly intensities are defined relative to  $\sigma_0$ , preventing uncontrolled amplification effects. Random seeds and diverse parameter sampling strategies are employed to guarantee robustness and reproducibility of results.

b) Scale and Sparsity Design: To systematically assess metric behavior under varying data scales and anomaly densities, a stratified sampling design is adopted with three control dimensions: sequence length, contamination rate, and repetition.

Sequence lengths are set to 5k, 10k, and 50k, corresponding to short, medium, and long time series scenarios. Anomaly

segment lengths and local window parameters are scaled proportionally to maintain comparability. Contamination rates are set to 5%, 10%, 15%, and 20%, covering sparse, moderate, and dense anomaly distributions. For repetition, each (length  $\times$  contamination  $\times$  random seed) combination is independently generated 60 times to control stochastic variation and ensure statistical confidence.

## B. Prediction Strategies and Control Groups

This section introduces the prediction and control strategies used to validate the robustness of metrics. The core idea is to construct a continuous degradation sequence from high-quality predictions to purely random ones (termed the *quality gradient*), enabling systematic comparison of metric responses under both informative and spurious detection conditions.

This design tests two essential properties:

- 1) whether a metric correctly reflects detection quality differences (monotonicity);
- whether it can effectively distinguish informative predictions from random noise (anti-randomness).
- a) Genuine Detector Group: To represent "informative detectors," three representative time series models are selected: **DLinear**, **DeepAR**, and **Informer**. These cover distinct modeling paradigms:
  - *DLinear* an efficient linear residual model capturing trend and seasonal components in stationary series;
  - DeepAR a probabilistic autoregressive model capable of handling inter-series uncertainty;
  - *Informer* an attention-based model leveraging sparse self-attention for long sequence forecasting.

All models follow standardized training procedures with fixed hyperparameters (learning rate, epochs, sliding window length, etc.) to ensure reproducibility. If model outputs are point-wise predictions  $\hat{y}_t$ , anomaly scores are computed as:

$$s_t = \frac{|y_t - \hat{y}_t|}{\sigma_{\text{local}}},$$

and optionally normalized via residual quantile mapping or smoothing (e.g., Sigmoid) for comparability across models. This unified transformation ensures that differences in metric results reflect the evaluation framework itself rather than model-specific scale variations.

b) Quality Gradient Mechanism: To examine sensitivity and monotonic response, a Quality Gradient mechanism is designed to generate progressively degraded predictions. Controlled perturbations gradually reduce the alignment between predictions and ground truth, yielding a sequence of prediction qualities  $\alpha \in \{0.9, 0.8, \ldots, 0.1\}$ .

Prediction degradation is controlled by flipping ratios and noise amplitude:

- high-quality region ( $\alpha > 0.7$ ): mild perturbation,
- medium-quality region (0.4 <  $\alpha \le 0.7$ ): moderate noise and flipping,
- low-quality region ( $\alpha \leq 0.4$ ): transition to random Bernoulli predictions.

When  $\alpha \leq 0.2$ , predictions become completely uninformative, forming a random baseline.

The monotonicity of each metric is quantified by the Spearman rank correlation coefficient  $\rho$  between metric scores and quality levels. A significantly positive  $\rho$  close to 1 indicates stable monotonic behavior, whereas  $\rho \approx 0$  or negative implies poor quality sensitivity.

- c) Random Prediction Groups (Control): To test resistance against "uninformative" or "pseudo-structured" predictions, three types of random prediction strategies are designed:
  - Uniform Score Random Scores are sampled from U(0,1) with expected anomaly rate  $p=\mathbb{E}[y_t]$ , and top-k positions are selected as alarms, reflecting baseline randomness.
  - Clustered Random Alarms are generated via a Poisson-cluster process to simulate spurious structural noise.
  - Pure Bernoulli Random Binary alarms  $a_t \sim \text{Bernoulli}(p)$  are independently sampled, representing fully uncorrelated randomness.

Each random strategy is repeated 20 times to estimate empirical score distributions. If a metric yields similar scores for genuine and random predictions, its robustness is insufficient. Conversely, if significant differences exist (quantified by AUC and Cohen's d), the metric demonstrates strong antirandomness and discriminative power.

To further assess gaming resistance, an **Oracle Attack** mechanism is introduced, simulating an adversarial detector that knows ground truth and manipulates predictions to maximize the target metric. A hill-climbing search is applied under an alarm-rate constraint  $\|\hat{y}\|_1 \leq \alpha L$  ( $\alpha = 0.1$ ) to iteratively perturb predictions for maximizing  $M(y,\hat{y})$ . If a metric can be easily inflated through such manipulation, its evaluation reliability is questionable. Final anomaly scores are sampled as:

$$s_t \sim \begin{cases} U(0.7, 1.0), & \text{if } \hat{y}_t = 1, \\ U(0.0, 0.3), & \text{otherwise.} \end{cases}$$

## C. Evaluation Metrics

The goal of this experiment is not to assess detector performance but to verify whether evaluation metrics can effectively distinguish informative detectors from random guessing. Three complementary quantitative dimensions are used: Average Cohen's effect size d, Average AUC, and Monotonicity coefficient  $(\rho)$ . These collectively form a comprehensive framework to assess discriminability, robustness, and interpretability.

a) Average Cohen's effect size d: To quantify the sensitivity of each metric to score differences between genuine detectors and random predictors, we compute the standardized mean difference:

$$d = \frac{\mu_{\text{genuine}} - \mu_{\text{random}}}{\sigma_{\text{pooled}}},$$

where  $\mu_{\rm genuine}$  and  $\mu_{\rm random}$  denote the mean scores of genuine and random predictors, respectively, and  $\sigma_{\rm pooled}$  is their pooled standard deviation. Larger d values indicate stronger discriminative capability.

Metric	Avg Effect Size	Avg AUC	Avg Genuine Score	Avg Random Score	Monotonicity
$AF_{\beta}$	18.309	1.000	0.853	0.675	0.713
Best- $PwF$	17.940	1.000	0.444	0.216	0.749
$CF_{\beta}$	17.239	1.000	0.563	0.201	0.728
$VUS^l$ - $PR$	15.638	1.000	0.392	0.128	0.719
P@K	14.415	1.000	0.413	0.123	0.715
$PwF_{\beta}$	14.415	1.000	0.413	0.123	0.701
AUC- $PR$	14.291	1.000	0.405	0.124	0.726
$SF_{eta}$	13.649	1.000	0.393	0.046	0.701
$RF^{\alpha}_{\beta}(front)$	13.373	1.000	0.528	0.156	0.722
$TaF^{\delta}_{\beta}$	13.351	1.000	0.495	0.105	0.694
$RF^{\alpha}_{\beta}(flat)$	12.952	1.000	0.516	0.156	0.735
$K\%$ - $PAF_{\beta}^{k}$	12.965	0.966	0.558	0.216	0.721
$VUS^l$ - $ROC$	12.797	1.000	0.727	0.488	0.760
$eTaF_{\beta}$	12.705	1.000	0.435	0.145	0.714
$AUC ext{-}ROC$	12.508	1.000	0.717	0.500	0.744
$TF^{ au}_{eta}$	12.413	1.000	0.556	0.258	0.715
$LSF^w$	11.575	1.000	0.677	0.482	0.712
TD	5.826	0.938	0.966	0.912	0.696
$dT$ - $PAF_{\beta}^{k}$	3.994	0.997	0.675	0.426	0.697
$PAF_{\beta}$	3.986	0.784	0.702	0.664	0.721
$PATE^{\varepsilon\delta}(F1)$	3.686	0.954	0.328	0.100	0.727
NAB	0.669	0.611	0.646	0.491	0.049

TABLE II
COMPARISON OF EVALUATION METRICS PERFORMANCE (SORTED BY AVG EFFECT SIZE DESCENDING)

- b) Average AUC: To further evaluate global separability, we treat metric scores as decision functions and compute the area under the ROC curve (AUC), where random samples are labeled as 0 (negative) and genuine detectors as 1 (positive). AUC values range from 0.5 (no discrimination) to 1.0 (perfect discrimination).
- c) Monotonicity Coefficient ( $\rho$ ): To assess the consistency of metric response to detection quality, the Spearman rank correlation coefficient  $\rho$  between metric scores and quality levels is computed. Following empirical thresholds,  $\rho \geq 0.8$  indicates strong monotonicity, whereas  $\rho < 0.2$  suggests no significant monotonic relationship.

### D. Experimental Results

To intuitively illustrate the distributional differences, Table II and Figures 4–5 summarize the main quantitative and visual results, including: (1) heatmaps of AUC and effect size, (2) score distributions ranked by composite performance, and (3) box–scatter plots jointly comparing effect size and AUC. The guiding principle is as follows: if a metric exhibits large, stable, and consistent differences between the score distributions of "genuine detectors" and "random predictors," it can be considered a valid reflection of detection quality; otherwise, such metrics should be used cautiously or only as part of a composite evaluation framework.

All experiments were independently repeated five times to reduce the impact of sample randomness. As shown in Figure 4, most metrics exhibit extremely high effect sizes (e.g., the average effect size of Best-PwF reaches approximately 19), with AUC values close to 1 across most datasets (darker regions on the right side of the heatmap). In the boxplots, the green boxes (representing genuine detectors)

are consistently and significantly higher than the red boxes (random predictions), with minimal overlap, indicating that random guessing almost never achieves comparable scores to genuine models. These results demonstrate that most metrics can reliably and significantly distinguish genuine detection from random guessing.

In contrast, metrics such as  $PaF_{\beta}$ ,  $PATE^{\epsilon\delta}$ , and especially NAB show noticeably weaker discriminative ability. For instance, in the case of  $PaF_{\beta}$ , the average scores of genuine and random predictors are close (0.702 vs. 0.664), with an effect size of only about 3.98 and an AUC of roughly 0.784. The situation is even worse for NAB, whose effect size and AUC are both low, and the monotonicity coefficient drops to approximately  $\rho=0.049$ . This indicates that, under the random baseline setting, this metric cannot reliably differentiate noise from meaningful detection results. Consequently, these metrics should be interpreted with caution, preferably used jointly with more robust metrics, or avoided as standalone evaluation criteria.

Additionally, as illustrated by the orange distributions in Figure 3, we also present the score distributions under *oracle attack* conditions (serving as a stress test to reveal potential "gaming" upper bounds). Overall, several metrics—particularly those sensitive to anomaly length or boundary coverage—can approach genuine detector scores under oracle optimization. This suggests that, in practice, certain metrics may be artificially inflated through targeted optimization. Although the oracle results are not used as formal evaluation evidence, they serve as an essential indicator of potential robustness risks.

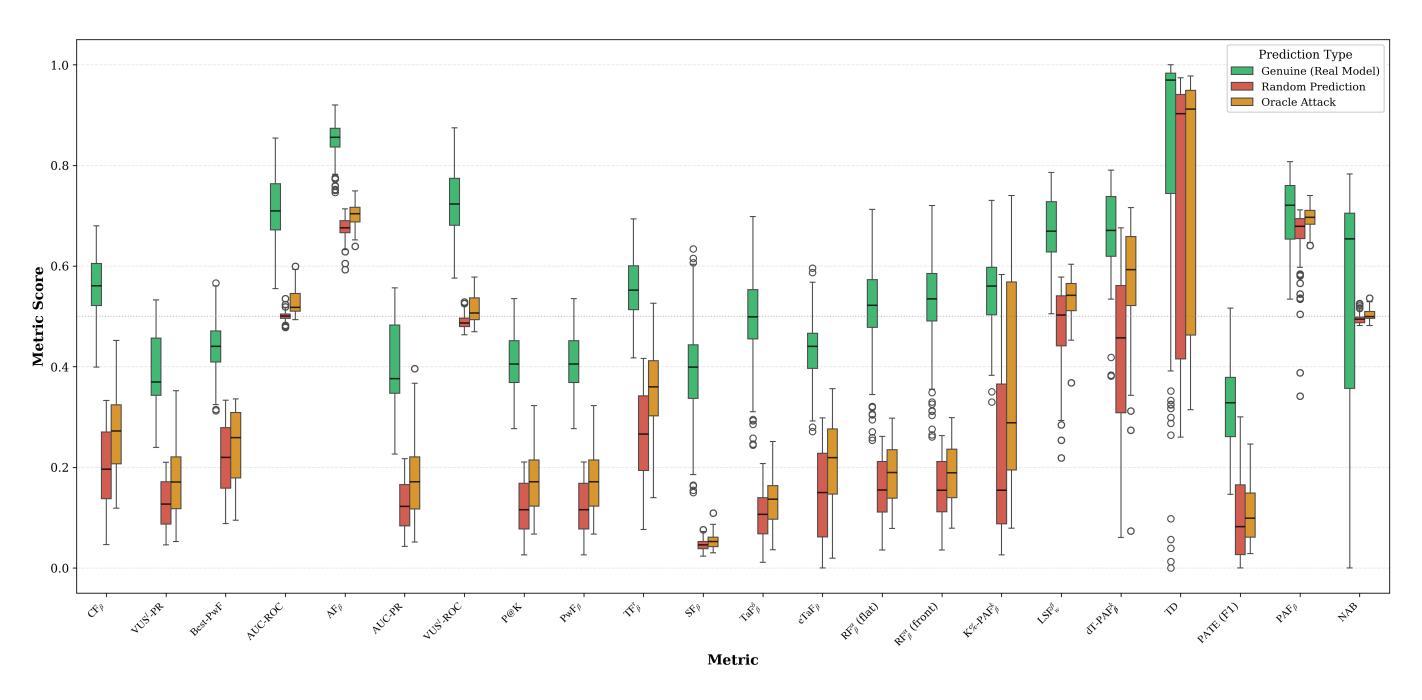


Fig. 3. Distribution of metric scores under genuine detectors, random guessing, and oracle-based attacks. Metrics whose genuine and random score distributions largely overlap are considered less robust and should be used cautiously or in combination with other stable metrics. Note that since the score ranges of TD and NAB differ from typical F1-based metrics (not bounded within [0, 1]), the NAB scores are normalized to [0, 1], and the TD scores are inversely normalized because smaller distances indicate better performance.

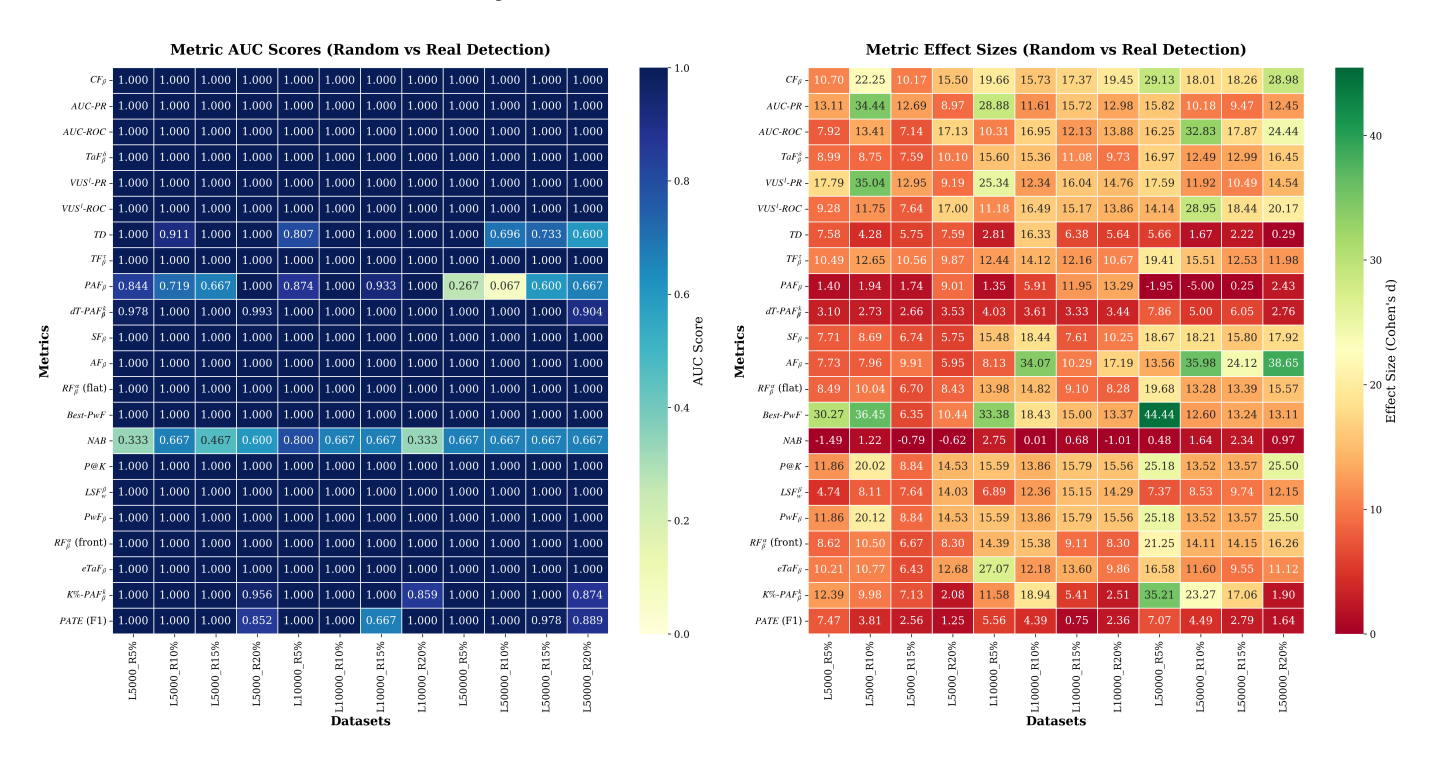


Fig. 4. Comprehensive comparison of 20+ time series anomaly detection metrics based on average effect size, AUC, genuine/random scores, and monotonicity. Higher intensity indicates stronger separability between genuine and random detection results. Here, Rn% denote datasets with overall anomaly ratios of n%, respectively, where each anomaly set contains diverse anomaly types.

#### V. CONCLUSION

This study presents a **problem-oriented framework for evaluating time series anomaly detection metrics**, aiming to bridge the gap between metric formulation and the specific challenges faced in practical anomaly detection tasks. Rather than categorizing metrics merely by their mathematical

expressions or evaluation levels, this framework classifies them according to the *underlying problems they are designed to address*. By reorganizing existing metrics into six major dimensions—basic evaluation, timeliness rewards, tolerance to annotation uncertainty, human-audit cost penalties, robustness against random or sparse predictions, and parameter-

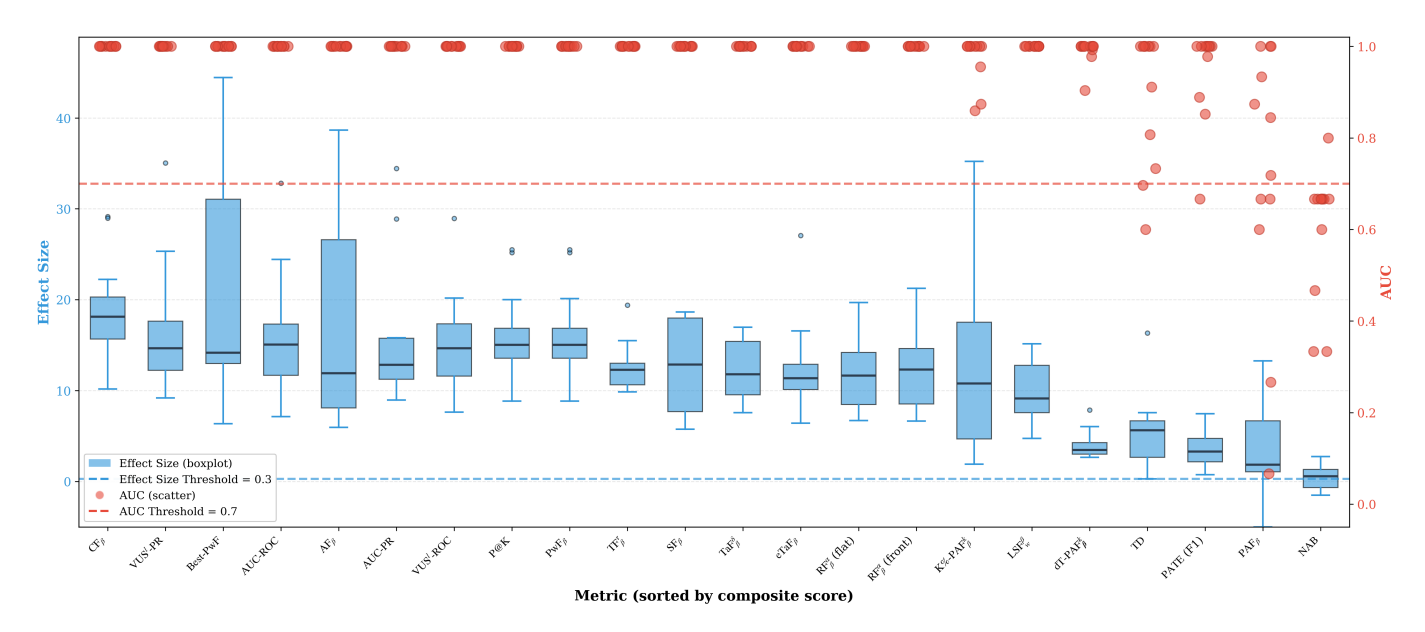


Fig. 5. Joint analysis of effect size and AUC across all metrics. Metrics located in the left region exhibit high discriminative ability, clearly separating genuine and random scores, while those near the right indicate weak robustness to random guessing.

free comparability—our analysis reveals the distinct design rationales and implicit trade-offs among them.

Through this problem-oriented perspective, we uncover that many existing evaluation inconsistencies originate from mismatched design intentions rather than mathematical deficiencies. Our framework highlights that the **choice of metric should be inherently task-dependent**, reflecting the real-world trade-offs between timeliness, reliability, interpretability, and auditability. Moreover, it offers a conceptual foundation for developing *next-generation evaluation metrics* that can dynamically adapt to evolving application needs—balancing precision, cost, and decision uncertainty in a principled manner.

Looking forward, future research could focus on formalizing a **multi-objective evaluation standard** that jointly considers temporal tolerance, cost asymmetry, and uncertainty calibration

By rethinking metric evaluation from a problem-driven standpoint, this work contributes a unified perspective that not only clarifies existing metric diversity but also inspires the principled design of more context-aware, equitable, and operationally meaningful evaluation systems for time series anomaly detection.

#### REFERENCES

- A. A. Cook, G. Mısırlı, and Z. Fan, "Anomaly detection for iot timeseries data: A survey," *IEEE Internet of Things Journal*, vol. 7, no. 7, pp. 6481–6494, 2019.
- [2] S. Lucero *et al.*, "Iot platforms: enabling the internet of things," *White paper*, 2016.
- [3] E. Estopace, "Idc forecasts connected iot devices to generate 79.4 zb of data in 2025," *FutureloT, June*, 2019.
- [4] C. Feng and P. Tian, "Time series anomaly detection for cyber-physical systems via neural system identification and bayesian filtering," in Proceedings of the 27th ACM SIGKDD Conference on Knowledge Discovery & Data Mining, 2021, pp. 2858–2867.

- [5] Z. Fang, Y. Yang, S. Wang, B. Fu, Z. Song, F. Zhang, and D. Zhang, "Mac: Measuring the impacts of anomalies on travel time of multiple transportation systems," *Proceedings of the ACM on Interactive, Mobile, Wearable and Ubiquitous Technologies*, vol. 3, no. 2, pp. 1–24, 2019.
- [6] M. Ma, S. Zhang, J. Chen, J. Xu, H. Li, Y. Lin, X. Nie, B. Zhou, Y. Wang, and D. Pei, "{Jump-Starting} multivariate time series anomaly detection for online service systems," in 2021 USENIX Annual Technical Conference (USENIX ATC 21), 2021, pp. 413–426.
- [7] D. S. Stoffer and H. Ombao, "Special issue on time series analysis in the biological sciences," pp. 701–703, 2012.
- [8] J. E. Zhang, D. Wu, and B. Boulet, "Time series anomaly detection for smart grids: A survey," in 2021 IEEE Electrical Power and Energy Conference (EPEC). IEEE, 2021, pp. 125–130.
- [9] Y. Zhou, J. Jiang, S.-H. Yang, L. He, Y. Ding, K. Liu, G. Zhu, and Y. Qing, "A data-distillation-enhanced autoencoder for detecting anomalous gas consumption," *IEEE Internet of Things Journal*, vol. 11, no. 2, pp. 3473–3483, 2023.
- [10] E. Keogh, J. Lin, A. Fu, and H. Van Herle, "Finding unusual medical time-series subsequences: Algorithms and applications," *IEEE Trans*actions on Information Technology in Biomedicine, vol. 10, no. 3, pp. 429–439, 2006.
- [11] S. Baireddy, S. R. Desai, J. L. Mathieson, R. H. Foster, M. W. Chan, M. L. Comer, and E. J. Delp, "Spacecraft time-series anomaly detection using transfer learning," in 2021 IEEE/CVF Conference on Computer Vision and Pattern Recognition Workshops (CVPRW). IEEE, 2021, pp. 1951–1960.
- [12] S. Crépey, N. Lehdili, N. Madhar, and M. Thomas, "Anomaly detection in financial time series by principal component analysis and neural networks," *Algorithms*, vol. 15, no. 10, p. 385, 2022.
- [13] G. Box, "Box and jenkins: time series analysis, forecasting and control," in A Very British Affair: Six Britons and the Development of Time Series Analysis During the 20th Century. Springer, 2013, pp. 161–215.
- [14] L. Ruff, R. Vandermeulen, N. Goernitz, L. Deecke, S. A. Siddiqui, A. Binder, E. Müller, and M. Kloft, "Deep one-class classification," in *International conference on machine learning*. PMLR, 2018, pp. 4393–4402.
- [15] B. Zong, Q. Song, M. R. Min, W. Cheng, C. Lumezanu, D. Cho, and H. Chen, "Deep autoencoding gaussian mixture model for unsupervised anomaly detection," in *International conference on learning representa*tions, 2018.
- [16] H. Xu, Y. Wang, S. Jian, Q. Liao, Y. Wang, and G. Pang, "Calibrated one-class classification for unsupervised time series anomaly detection," *IEEE Transactions on Knowledge and Data Engineering*, vol. 36, no. 11, pp. 5723–5736, 2024.
- [17] S. S. Saravanan, Time series anomaly detection using generative adversarial networks. Missouri University of Science and Technology, 2023.

[18] V. Chandola, A. Banerjee, and V. Kumar, "Anomaly detection: A survey," ACM computing surveys (CSUR), vol. 41, no. 3, pp. 1–58, 2009.

- [19] L. Zhang, J. Zhu, G. Han, B. Jin, P. Wang, and X. Wei, "Self-supervised disentangled representation learning for time series anomaly detection," *IEEE Internet of Things Journal*, 2025.
- [20] S. Qin, L. Chen, Y. Luo, and G. Tao, "Multiview graph contrastive learning for multivariate time-series anomaly detection in iot," *IEEE Internet of Things Journal*, vol. 10, no. 24, pp. 22401–22414, 2023.
- [21] H. Zhu, C. Yi, S. Rho, S. Liu, and F. Jiang, "An interpretable multivariate time-series anomaly detection method in cyber–physical systems based on adaptive mask," *IEEE Internet of Things Journal*, vol. 11, no. 2, pp. 2728–2740, 2024.
- [22] L. Fu, M. Ma, and Z. Zhai, "Deep koopman predictors for anomaly detection of complex iot systems with time series data," *IEEE Internet* of *Things Journal*, vol. 11, no. 23, pp. 38360–38369, 2024.
- [23] Z. Chen, D. Chen, X. Zhang, Z. Yuan, and X. Cheng, "Learning graph structures with transformer for multivariate time-series anomaly detection in iot," *IEEE Internet of Things Journal*, vol. 9, no. 12, pp. 9179–9189, 2022.
- [24] K. Hundman, V. Constantinou, C. Laporte, I. Colwell, and T. Soderstrom, "Detecting spacecraft anomalies using lstms and nonparametric dynamic thresholding," in *Proceedings of the 24th ACM SIGKDD International Conference on Knowledge Discovery & Data Mining*, 2018, pp. 387–395.
- [25] S. Sørbø and M. Ruocco, "Navigating the metric maze: A taxonomy of evaluation metrics for anomaly detection in time series," *Data Mining* and Knowledge Discovery, vol. 38, no. 3, pp. 1027–1068, 2024.
- [26] M. A. Bashar and R. Nayak, "Tanogan: Time series anomaly detection with generative adversarial networks," in 2020 IEEE Symposium Series on Computational Intelligence (SSCI). IEEE, 2020, pp. 1778–1785.
- [27] S. Han and S. S. Woo, "Learning sparse latent graph representations for anomaly detection in multivariate time series," in *Proceedings of* the 28th ACM SIGKDD Conference on Knowledge Discovery and Data Mining. ACM, 2022, pp. 2977–2986.
- [28] Z. Li, Y. Zhao, J. Han, Y. Su, R. Jiao, X. Wen, and D. Pei, "Multivariate time series anomaly detection and interpretation using hierarchical intermetric and temporal embedding," in *Proceedings of the 27th ACM SIGKDD Conference on Knowledge Discovery & Data Mining*. ACM, 2021, pp. 3220–3230.
- [29] A. Abdulaal, Z. Liu, and T. Lancewicki, "Practical approach to asynchronous multivariate time series anomaly detection and localization," in *Proceedings of the 27th ACM SIGKDD Conference on Knowledge Discovery & Data Mining*. ACM, 2021, pp. 2485–2494.
- [30] D. Berrar and P. Flach, "Caveats and pitfalls of roc analysis in clinical microarray research (and how to avoid them)," *Briefings in Bioinformatics*, vol. 13, no. 1, pp. 83–97, 2012.
- [31] A. Garg, W. Zhang, J. Samaran, R. Savitha, and C.-S. Foo, "An evaluation of anomaly detection and diagnosis in multivariate time series," *IEEE Transactions on Neural Networks and Learning Systems*, vol. 33, no. 6, pp. 2508–2517, 2022.
- [32] R.-Q. Chen, G.-H. Shi, W.-L. Zhao, and C.-H. Liang, "A joint model for it operation series prediction and anomaly detection," *Neurocomputing*, vol. 448, pp. 130–139, 2021.
- [33] A. Lavin and S. Ahmad, "Evaluating real-time anomaly detection algorithms the numenta anomaly benchmark," in 2015 IEEE 14th International Conference on Machine Learning and Applications (ICMLA). IEEE, 2015, pp. 38–44.
- [34] N. Tatbul, T. J. Lee, S. Zdonik, M. Alam, and J. Gottschlich, "Precision and recall for time series," in *Advances in Neural Information Processing Systems*, vol. 31. Curran Associates, Inc., 2018.
- [35] E. Scharwächter and E. Müller, "Statistical evaluation of anomaly detectors for sequences," 2020.
- [36] G. Kovács, G. Sebestyen, and A. Hangan, "Evaluation metrics for anomaly detection algorithms in time-series," *Acta Universitatis Sapi*entiae, Informatica, vol. 11, no. 2, pp. 113–130, 2019.
- [37] A. Huet, J. M. Navarro, and D. Rossi, "Local evaluation of time series anomaly detection algorithms," in *Proceedings of the 28th ACM SIGKDD Conference on Knowledge Discovery and Data Mining*. ACM, 2022, pp. 635–645.
- [38] W.-S. Hwang, J.-H. Yun, J. Kim, and H. C. Kim, "Time-series aware precision and recall for anomaly detection: Considering variety of detection result and addressing ambiguous labeling," in *Proceedings of the 28th ACM International Conference on Information and Knowledge Management*. ACM, 2019, pp. 2241–2244.
- [39] W.-S. Hwang, J.-H. Yun, J. Kim, and B. G. Min, ""do you know existing accuracy metrics overrate time-series anomaly detections?"," in Pro-

- ceedings of the 37th ACM/SIGAPP Symposium on Applied Computing. ACM, 2022, pp. 403–412.
- [40] J. Paparrizos, P. Boniol, T. Palpanas, R. S. Tsay, A. Elmore, and M. J. Franklin, "Volume under the surface: A new accuracy evaluation measure for time-series anomaly detection," *Proceedings of the VLDB Endowment*, vol. 15, no. 11, pp. 2774–2787, 2022.
- [41] R. Ghorbani, M. J. Reinders, and D. M. Tax, "Pate: Proximity-aware time series anomaly evaluation," in *Proceedings of the 30th ACM SIGKDD Conference on Knowledge Discovery and Data Mining*, 2024, pp. 872–883.
- [42] J. Paparrizos, Y. Kang, P. Boniol, R. S. Tsay, T. Palpanas, and M. J. Franklin, "Tsb-uad: An end-to-end benchmark suite for univariate time-series anomaly detection," *Proceedings of the VLDB Endowment*, vol. 15, no. 8, pp. 1697–1711, 2022.
- [43] S. Kim, K. Choi, H.-S. Choi, B. Lee, and S. Yoon, "Towards a rigorous evaluation of time-series anomaly detection," *Proceedings of the AAAI Conference on Artificial Intelligence*, vol. 36, no. 7, pp. 7194–7201, 2022
- [44] S. Liu, B. Zhou, Q. Ding, B. Hooi, Z. Zhang, H. Shen, and X. Cheng, "Time series anomaly detection with adversarial reconstruction networks," *IEEE Transactions on Knowledge and Data Engineering*, vol. 35, no. 4, pp. 4293–4306, 2023.
- [45] S. Bhatia, A. Jain, P. Li, R. Kumar, and B. Hooi, "Mstream: Fast anomaly detection in multi-aspect streams," in *Proceedings of the Web Conference* 2021. ACM, 2021, pp. 3371–3382.
- [46] T. Kieu, B. Yang, C. Guo, and C. S. Jensen, "Outlier detection for time series with recurrent autoencoder ensembles," in *Proceedings of the Twenty-Eighth International Joint Conference on Artificial Intelligence*. International Joint Conferences on Artificial Intelligence Organization, 2019, pp. 2725–2732.
- [47] D. Park, Y. Hoshi, and C. C. Kemp, "A multimodal anomaly detector for robot-assisted feeding using an lstm-based variational autoencoder," *IEEE Robotics and Automation Letters*, vol. 3, no. 3, pp. 1544–1551, 2018.
- [48] E. Dai and J. Chen, "Graph-augmented normalizing flows for anomaly detection of multiple time series," arXiv preprint arXiv:2202.07857, 2022
- [49] T. Ergen and S. S. Kozat, "Unsupervised anomaly detection with 1stm neural networks," *IEEE Transactions on Neural Networks and Learning Systems*, vol. 31, no. 8, pp. 3127–3141, 2020.
- [50] A. Goodge, B. Hooi, S. K. Ng, and W. S. Ng, "Robustness of autoencoders for anomaly detection under adversarial impact," in *Proceedings* of the twenty-ninth international conference on international joint conferences on artificial intelligence, 2021, pp. 1244–1250.



Kaixiang Yang Kaixiang Yang received the B.S. degree in metallic materials engineering from Nanjing Tech University, China, in 2023. He is currently working toward the M.S. degree with the College of AI, Yunnan University, China. His research interests include time series data analysis, artificial intelligence, pattern recognition, and machine learning.



Jiarong Liu Jiarong Liu received the B.S. degree in software engineering from Guangdong Ocean University, China, in 2023. He is currently working toward the M.S. degree with the College of AI, Yunnan University, China. His research interests include time series data analysis, artificial intelligence, pattern recognition, and machine learning.



Yupeng Song Yupeng Song is currently a Lecturer at the School of Software and the School of Engineering, Yunnan University, China. He received his degree from the School of Computer Science at Wuhan University in 2024. His research interests include artificial intelligence, computer vision, and computer graphics.



Shuanghua Yang Shuanghua Yang is currently a Chair Professor in the Institute for Advanced Study at Beijing Normal–Hong Kong Baptist University, Zhuhai, China. He was selected as a member of the European Academy of Sciences and Arts in 2024 and awarded a DSc from Loughborough University in 2014 to recognize his academic contribution to wireless monitoring research. He is a Fellow of the IET and a Fellow of InstMC, U.K. His current research interests include cyber-physical system safety and security, and the industrial Internet of Things.



Yujue Zhou Yujue Zhou received the B.S. degree from Zhejiang University, China, in 2015, the M.S. degree (with distinction) from the University of Warwick, U.K., in 2018, and the Ph.D. degree in computer science from the University of Warwick, U.K., in 2023. She is currently a Lecturer in the AI College of Yunnan University, China. Her current research interests include time series data analysis, artificial intelligence, pattern recognition, and machine learning.